THESIS FOR THE DEGREE OF DOCTOR OF PHILOSOPHY

Submicron gas bubbles in water

FREDRIK EKLUND

Department of Physics

CHALMERS UNIVERSITY OF TECHNOLOGY

Gothenburg, Sweden 2020

Submicron gas bubbles in water

FREDRIK EKLUND

ISBN 978-91-7905-349-9

Doktorsavhandlingar vid Chalmers tekniska högskola

Ny serie nr 4816

ISSN 0346-718X

Department of Physics

Chalmers University of Technology

SE-412 96 Gothenburg

Sweden

Telephone + 46 (0)31-772 1000

Cover:

The authors rendition of laser holography and light scattering.

The green laser beam is being scattered by a bubble.

The red laser beam speeds up when passing through an air bubble, whereas the speed of light is lower in water.

The resulting phase shift can be detected by digital holography.

Based on a bubble image from Vectorstock, NZ.

Chalmers Digitaltryck

Gothenburg, Sweden 2020

Submicron gas bubbles in water

Fredrik Eklund
Department of Physics
Chalmers University of Technology
SE-412 96 Gothenburg
Sweden

Abstract

Gas bubbles smaller than 1 micrometre in water, commonly referred to as nanobubbles, is a growing field of research and innovation. Applications range from medical imaging and drug delivery to mining industry and environmental remediation. Despite much activity, important questions remain – which are the mechanisms that allow small gas bubbles to be stable against dissolution and are stable nanobubbles really as common and easily generated as is often claimed?

This work demonstrates that several common nanobubble generation methods can generate particle agglomerates or oil droplets which can be mistaken for bubbles, whereas stable nano- and microbubbles are less easy to generate than commonly believed. The results further suggest that stable bubbles are normally stable due to a shell of surface-active organic compounds, whereas other proposed stability mechanisms are less likely. An unexpected finding was that sorbitan surfactant stabilized air nanobubbles can form long-lived bubble agglomerates.

Holographic Nanoparticle Tracking Analysis (H-NTA) is demonstrated as a powerful new method to detect and differentiate between bubbles and particles in the same dispersion. As H-NTA determines the refractive index of tracked objects, bubbles will differ very significantly from solid particles or oil droplets. The method also enables detection of different populations of particles, agglomerates and oil droplets in the same dispersion.

Keywords: nanobubbles, microbubbles, ultrafine bubbles, nanoparticle tracking analysis, digital holographic microscopy

Appended papers

Paper I. Stable air nanobubbles in water - the importance of organic contaminants

Fredrik Eklund, Jan Swenson

Langmuir 2018, 34, 11003-11009

Paper II. Size and refractive index determination of Subwavelength Particles and Air Bubbles by Holographic Nanoparticle Tracking Analysis

Daniel Midtvedt, Fredrik Eklund, Erik Olsén, Benjamin Midtvedt, Jan Swenson, Fredrik Höök

Analytical Chemistry 92, 1908-1915 (2020)

Paper III. Experimental evaluation of the dynamic equilibrium model for stable air nanobubbles in water

Fredrik Eklund, Adrian Eriksson, Fredrik Höök, Jan Swenson

Submitted.

Paper IV. The stability and dynamics of sorbitan surfactant stabilized air nanobubbles investigated with Holographic Nanoparticle Tracking Analysis (H-NTA)

Fredrik Eklund, Daniel Midtvedt, Erik Olsén, Fredrik Höök, Jan Swenson.

In manuscript.

Paper not included in the thesis

Holographic characterisation of subwavelength particles enhanced by deep learning

Benjamin Midtvedt, Erik Olsén, Fredrik Eklund, Fredrik Höök, Caroline Beck Adiels, Giovanni Volpe, Daniel Midtvedt

Submitted. Preprint: ArXiv 2006.11154

My contributions to the appended papers

Paper I.

I suggested and performed all experimental work and was the main author of the manuscript.

Paper II.

I suggested and prepared the samples and performed the reported measurements. I also contributed to developing the method, primarily as a user and by improving the experimental setup. I wrote a substantial part of the manuscript, in particular the bubble related sections. Shared first-authorship.

Paper III.

I suggested the experimental work and performed a large part of it. I was the main author of the manuscript.

Paper IV.

I suggested and performed all experimental work and was the main author of the manuscript.

List of terms and abbreviations

DHM	Digital Holographic Microscopy
NTA	Nanoparticle Tracking Analysis
H-NTA	Holographic Nanoparticle Tracking Analysis
DLS	Dynamic Light Scattering
PTFE	Polytetrafluoroethylene (a.k.a. Teflon)
Lipid	Oily, water-insoluble substances found in living cells. Often surface-active.
Surfactant	Surface-active substance, term mostly used for synthetic substances

Table of contents

1 Introduction

Micro- and nanobubbles in water is a rapidly growing research topic. The interest is fuelled mostly by the many existing and potential technical and medical applications and there is plenty of industrial innovation activity in this field. Microbubbles (fine bubbles) are used since many years as contrast agent in medical ultrasound imaging[1] and are now being explored also as a drug delivery vehicle. Industrially, microbubbles are used in water purification[2] and for separation processes in the mining industry[3]. In recent years, a large number of small innovation companies have developed different ways to generate smaller bubbles (ultrafine or nanobubbles) and explored new areas of use. Nanobubble technology has been applied in cleaning[4], fish farms and agriculture[5], environmental remediation[6], disinfection[7] and more. The possibilities seem endless and the future bright. However, the understanding of the properties of nanobubbles remains limited and sometimes there is even reason to doubt scientific reports as well as commercial claims.

Besides artificially generated bubbles, small gas bubbles do already exist in water naturally. These bubbles affect common phenomena such as cavitation and boiling. The existence of small gas bubbles in water has been known for a long time, in older literature these are referred to as “cavitation nuclei”. Water without any such “nuclei” behave considerably different from normal water in that formation of larger, macroscopic bubbles is considerably more difficult when gaseous “nuclei” are not present. Therefore, nuclei-free water can be heated to considerably higher temperatures than 100°C before bursting into a boil.

Another role which bubbles play in nature is in the gas exchange between the atmosphere and the ocean. Bubbles, small and large, have a large impact on the dissolution of atmospheric gases, including CO_2 in sea water and need therefore to be taken into account in research on climate and ocean acidification[8]. Recently, nanobubbles were suggested to be of vital importance in the life of trees[9]. The theory is that air released by the extreme sub-pressures in tree sap forms nanobubbles rather than macroscopic bubbles which would block the flow. As bubbles are present everywhere, they may play many more roles in nature which we are presently not aware of. Understanding nature thus provides a second motivation for the study of very small bubbles.

Whereas many technical designs for “bubble generators” have been developed, there is still a fundamental lack of knowledge about the bubbles themselves and what factors are necessary for their stability. Theoretically, a very small air bubble in water should dissolve almost instantly, but something often stabilizes them for hours and days. This thesis is partially a search for this “something”.

Furthermore, the study of bubbles smaller than 1 μm faces some difficulties due to that detection and measurement of these bubbles is not entirely straightforward. Several commonly used methods for detection of particles in liquids cannot differentiate between particles, bubbles and droplets. Many methods have been suggested to differentiate between bubbles and particles, some of these have been explored in this work.

2 Historical and technical background

2.1 Overview

With improved light scattering instruments, many researchers discovered unexpected submicron particles in various aqueous solutions during the late 90s and early 2000s[10-13]. Such particles were sometimes interpreted as "solute clusters", loose aggregates of dissolved substances. Sometimes they were interpreted as "nanobubbles" of air. These interpretations were probably not always correct in either case. At the same time, Atomic Force Microscopy (AFM) became better and more affordable and scientists discovered submicron particles on hydrophobic surfaces in water, which were also interpreted as bubbles of air[14, 15]. Free floating "bulk nanobubbles" and interfacial- or surface nanobubbles initially progressed as two rather separate research areas. Surface nanobubbles initially received much more attention as they were easy to generate repeatably and to study with AFM, and probably also since the existence of bulk nanobubbles was more questioned. As early papers on "nanobubbles" rarely reference older literature on "cavitation nuclei", there seem to have been a common unawareness of it.

The new discovery of nanobubbles fuelled plenty of innovation activity both inside and outside academia. Soon several nanobubble generators were available on the market and new applications were explored by enthusiastic entrepreneurs. Much of this innovation activity took and takes place in Japan, where the Fine Bubble Industry Association (FBIA) was formed in 2012 and as of today has 80 corporate members[16]. FBIA has initiated a comprehensive standardization work in the International Standardization Organization (ISO). One of the results from the work within ISO Technical committee 281 is a recommendation that the term "nanobubble" for bubbles smaller than 1 micron be replaced with "ultrafine bubble" as the term "nano" is generally recommended to be used for objects smaller than 100nm. For bubbles in the range 1 to 100 micron, the term "fine bubble" is recommended. In scientific literature the terms nanobubble and microbubble are however still very common, and therefore used in this thesis. The term micro-nanobubbles is also used, meaning a mixture of micro- and nanobubbles which is often the output of commercial bubble generators.

2.2 Cavitation and boiling

Although it may seem like nanobubbles were discovered in the 1990ies, there have been strong indications of their existence much earlier. Cavitation is a phenomena where locally low pressure in water causes a vapor cavity to appear, expand and collapse. Cavitation can occur around propellers or in pumps and cause erosion of metallic materials when the bubble collapse takes place at the surface. Cavitation on ship propellers was discovered in the late 1800s, although the problem had been noticed in rotating machinery much earlier[17]. It was later found that cavitation in very pure water requires orders of magnitude greater sub-pressures to occur, compared to "normal" water[18, 19]. It can also be shown theoretically that the tensile strength of pure water is considerably higher than what is observed in "normal" water. By normal water is here meant for example tap water or any fresh water that has not been highly purified. Apparently, there is some kind of "cavitation nuclei" in normal water that facilitates cavitation. Harvey suggested that gas pockets reside in crevices in suspended particles and on surfaces[20]. Fox and Herzfield suggested in 1954 that microscopic air bubbles stabilised by an organic skin may act as a cavitation nuclei[21].

Early work with water tunnels (the equivalent of wind tunnels) found that cavitation nuclei rapidly accumulated due to cavitation and were recirculated to the tunnel entrance. A solution was found where a long return pipe at elevated pressure forced most of the "nuclei" to dissolve. Secondly, a deaerator reduced the air saturation to 20-50% in the water[22]. Many experiments in this field have shown that nuclei are often spherical and in the range of a few microns to a few hundred microns[17], but without determining their exact nature. Already in the 1960ies several researchers showed that the presence of a small concentration of organic substances in water influenced the cavitation threshold[23], which indicates that the nuclei are bubbles which are stabilized by organic surface active compounds. Also very recent studies in water tunnels[24, 25] suggest that nuclei responsible for hydrodynamic cavitation are made out of microbubbles in the 1-100μm range. The concentration varies over several orders of magnitude between different water tunnels, and is typically at or below 1/ml. In the case of hydrodynamic cavitation, i.e. cavitation in streaming water, the sub-pressures are relatively low, and therefore comparably large nuclei are required for cavitation to occur. It should be mentioned that hydrodynamic cavitation also can be nucleated by gaseous nuclei on surfaces, in particular hydrophobic surfaces.

Cavitation can also be induced by exposing water to ultrasound or mechanical pressure pulses. In this case higher sub pressures can be achieved and thus smaller gaseous nuclei are active. It has been experimentally shown that particles, carrying gas bubbles, can act as cavitation nuclei[26-28] in acoustic cavitation. Pressurization and degassing have been showed to inactivate such nuclei, and they are also depleted by cavitation events. This makes it obvious that the nuclei comprise gas bubbles in some form. In a recent study[28] on acoustic cavitation in particle dispersions, nuclei were found to spontaneously regenerate in about 10 min, which was assumed to be due to gas adsorption on the particles.

An early interesting finding was that cosmic radiation appears to generate stable cavitation nuclei. It had already been shown that a superheated liquid was sensitive to cosmic radiation and neutron sources[29]. Superheated ether was shown to burst into boiling faster in presence of a neutron source, and boiling was also shown to be triggered by cosmic radiation. This effect was soon put into use in "bubble chambers" for detection of high energy particles which generate a trace of macroscopic bubbles along their trajectory in liquified gas. Later, water was shown to be more resistant to sonically induced cavitation when shielded against neutron radiation[30], something which has been confirmed by several authors[31, 32] and shown in other liquids[31, 33]. The cavitation nuclei generated by neutron radiation appeared to have a half-time of about 70 minutes[30]. Interestingly enough, neutron radiation has also been shown to affect the bubble-mediated long range hydrophobic attraction[34] (see also chapter 3.6). The main mechanism is believed to be that neutrons collide with oxygen nuclei, which in their turn release energy locally as they slow down, causing local heating. In addition, neutrons themselves generate gamma- and alfa radiation along their path which both generate local heating and dissociation of water molecules (radiolysis) into hydrogen and oxygen.

Like cavitation, boiling is also affected by the presence of microscopic gas bubbles which are needed as nuclei for macroscopic vapor bubble formation. It was shown already more than 200 years ago that degassed water could be superheated considerably above 100°C before boiling, and the search for the "true" boiling point of water became a popular research subject at the time[35]. The surface material and cleanliness of the vessel was shown to be important, in addition to dissolved gas concentration. Very high superheating was achieved for water droplets suspended in oil. Boiling temperatures as high as 200°C have been reported[19, 35]. Superheating is fairly easy to achieve with pure

water and a microwave oven, since microwaves heats the water more uniformly than other common heating methods as well as enables the use of vessels with clean and smooth surfaces. Numerous accidents have been reported due to this phenomenon, as the superheated water can violently erupt once boiling starts.

2.3 Decompression sickness

A phenomenon similar to cavitation is the formation of air bubbles due to decompression. (The term cavitation is usually reserved for formation of vapor bubbles, rather than gas bubbles, although both phenomena may occur in conjunction.) This phenomenon can cause decompression sickness, also known as divers' disease, and is due to formation of gas bubbles in the body when traveling from a high pressure to a lower pressure environment. Bubbles can form at different places in the body and many different symptoms can therefore arise. Most common is joint pain, which is not unexpected since the joints are known to contain gas bubbles and thus nuclei for formation of larger bubbles. In the most serious cases, bubbles are released in the spinal cord and in the blood stream, leading to paralysis or death.

The gas supersaturation attainable in human blood is far too low for spontaneous bubble nucleation to occur. Pre-existing nuclei must be present[36]. Pressure treatment can destroy nuclei, which was proven in vivo on shrimp as well as rats. Exposure to high pressures before a decompression greatly reduced the number of bubbles formed and the incidence of decompression sickness. Bubble formation is believed not to take place in the cells or in the blood, but rather in places where gas is already regularly observed and where symptoms of decompression sickness are most common, namely the joints, including the spine[36]. Further evidence of this is that more bubbles seem to be generated when a suffering animal or person is moving. Arielli[37] did however observe bubble nucleation at the surface of blood vessels in water upon decompression and concluded that nucleation takes place from nuclei on hydrophobic surfaces.

Guidelines and tables for divers to avoid decompression sickness are based on empirical experience and animal testing. In later studies, bubble formation in Agarose gels was used as a model system, providing some interesting insights[38-41]. Just like in cavitation in water, bubble formation was found to depend on the presence of small gaseous nuclei. By filtering the distilled water used to prepare the gels through filters of different pore sizes, it could be concluded that the nuclei had a size from 1 μm down to less than 0.2 μm[42]. The number density appeared to increase with decreasing radius.

2.4 Contrast agents

Due to the ability of bubbles to resonate with high frequency sound, they absorb and scatter ultrasound very strongly. In the late 1960s, researchers working with ultrasound imaging noticed a strong contrast enhancement when certain solutions where injected into the blood stream. It was soon found that this was due to formation of microbubbles[43, 44]. The first commercial product appeared on the market in 1990 and was soon followed by several others[45, 46]. Early products were based on generation of air bubbles and had a very short half-life. Eventually air was replaced by fluorinated gases with very low water solubility. As these gases diffuse into the water much more slowly due to their limited solubility, this improved the half-life considerably. Other improvements for enhanced stability were the introduction of bubble shells of lipids, proteins and polymers. Microbubble contrast agents typically have a size distribution of 1-7 μm. In more recent research, microfluidic techniques have been explored for production of microbubbles as well as nanobubbles. One advantage of using smaller nanobubbles is that they can penetrate into tissue that microbubbles can not[47-49]. There is also great interest in the use of bubbles as a combined contrast agent and therapeutic agent / drug delivery vehicle[49, 50]. Several new types of contrast agents have also appeared in recent years, such as phase-change droplets and solid cavitation nucleating particles[51]. It should be stressed that compared to industrial nanobubbles, contrast agent/therapeutic bubbles is a very large research field with many published papers of high quality.

2.5 Flotation processes

Froth flotation is a very important process in the mining industry[3]. The process separates hydrophobic particles from hydrophilic particles based on the fact that hydrophobic particles adsorb on air bubbles which rise to the surface and create a froth. The process requires the material to be separated to be ground to a particle size of 0.1mm or less. Mined material (ore) is typically a mixture of different minerals and flotation is a powerful method to separate them. When the desired mineral is not naturally hydrophobic, chemicals are added which selectively adsorb to the mineral of interest and render it hydrophobic. In recent years, the use of nanobubbles in addition to regular larger bubbles has been explored[52-66]. The results indicate that enhanced flotation efficiency is possible.

Dissolved Air Flotation (DAF) is a different flotation technique which is commonly used for purification for drinking water and waste water[2, 67]. DAF is used to remove all solids from water whereas froth flotation is normally used

to separate different types of solids from each other. Whereas in froth flotation air is diffused directly into water, generating comparably large bubbles (>1mm), air is in DAF dissolved in water under pressure and bubbles of smaller size (<0.2 mm) are generated by depressurization and cavitation.

When applying nanobubbles in froth flotation, the mechanism has been suggested to be that bulk nanobubbles adsorb to and coat the surface of hydrophobic particles, which enhances their adsorption to larger bubbles. However, it may instead be that the nanobubble generation techniques used instead nucleate surface nanobubbles directly on the particles.

Adsorption of nanobubbles to hydrophobic particles can also be utilized in cleaning applications[4]. Adsorbed bubbles are in this case believed to keep dirt particles dispersed in solution, in a similar way as surfactants work. Commercial applications exist, such as washing machines or floor cleaning machines with integrated bubble generators, but cleaning with micro- and nanobubbles is a technology still in its infancy.

2.6 Agriculture, aquaculture and environmental remediation

Micro- and nanobubbles have successfully been used in agriculture[68], fish farming[5], in environmental remediation of soil and bottom sediments[6], and more[63]. In these applications, bubbles of pure oxygen are often used in addition to air bubbles, and the positive effects are probably to a large extent an effect of increased oxygen concentration in the water. It is claimed that micro- and nanobubbles due to their small size and long life have the ability to penetrate deep into bottom sediments and deliver oxygen, achieving results that conventional aeration techniques do not. In addition to bulk nanobubbles, bubble on surfaces and in pores of particles have been demonstrated for remediation of oxygen deficient sediments[6, 69, 70].

In addition to increased oxygen concentration, elevated concentrations of Reactive Oxygen Species (ROS) have also been detected in "nanobubble water"[7, 71]. ROS is most probably generated due to cavitation during the bubble production[72]. (ROS generation from collapse of stable nanobubbles has however been recently reported[73].) A collapsing cavitation bubble generates extreme pressures and temperatures which can enhance many chemical reactions, for example the production of ROS. The term ROS includes among others hydrogen peroxide, hydroxide radicals ($OH\cdot$) and superoxide radicals ($O2\cdot^{-}$). Through their oxidizing action these substances are harmful to living

organisms and can therefore work as disinfectants. However, at very low concentrations ROS actually stimulate cell growth and division and can therefore be beneficial[74]. Beneficial effects of nanobubbles in agriculture and aquaculture can thus be both due to increased oxygen levels and the generation of ROS. The ROS can stimulate growth of fish or plants at low concentrations as well as function as disinfectants at higher concentrations. At higher concentrations ROS can also be harmful to plants and animals, and harmful effects of nanobubble water have indeed been reported in some cases[7].

3 Theoretical background of nanobubbles

3.1 Gas diffusion

In a frequently quoted paper from 1950, Epstein and Plesset[75] calculated the expected life time of small air bubbles in water with the help of diffusion theory. The two driving forces for diffusion to or from a bubble are the saturation of gas in the water and the Laplace pressure. Laplace pressure is the pressure difference between the inside and outside of a gas bubble due to the surface curvature and the surface tension. The surface tension acts to pull the surface together, to decrease it, as illustrated in Fig. 1. This generates a force acting in parallel with the surface. When the surface is curved around an air bubble this will generate a net force acting towards the bubble. The internal pressure of the bubble generates an opposing force, balancing the force from the surface tension and the external pressure. The internal pressure of a bubble is thus the Laplace pressure plus the external pressure.

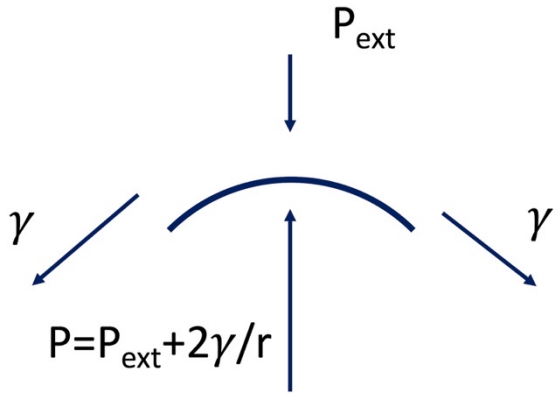

Fig. 1. Illustration of the pressure difference over a curved gas-water interface, caused by the surface tension, γ. r is the radius of curvature. P_{ext} is the external pressure in the liquid.

If an air –water interface is clean and does not have any surfactants adsorbed, the surface tension is very high (72 N/cm). If there is no surface tension at the air-water interface, a bubble will shrink when the water is undersaturated with air and grow if it is oversaturated. However, a small air bubble with a high surface tension will have a very high Laplace pressure which will force air to diffuse from the bubble into the water even at moderate oversaturation, as can be seen in Fig. 2. For a clean air bubble with 1μm diameter, the Laplace pressure will be high enough (2.9 bar) to drive dissolution at up to more than 150% saturation. Saturations up to about 150% are commonly occurring in natural waters or tap water[76].

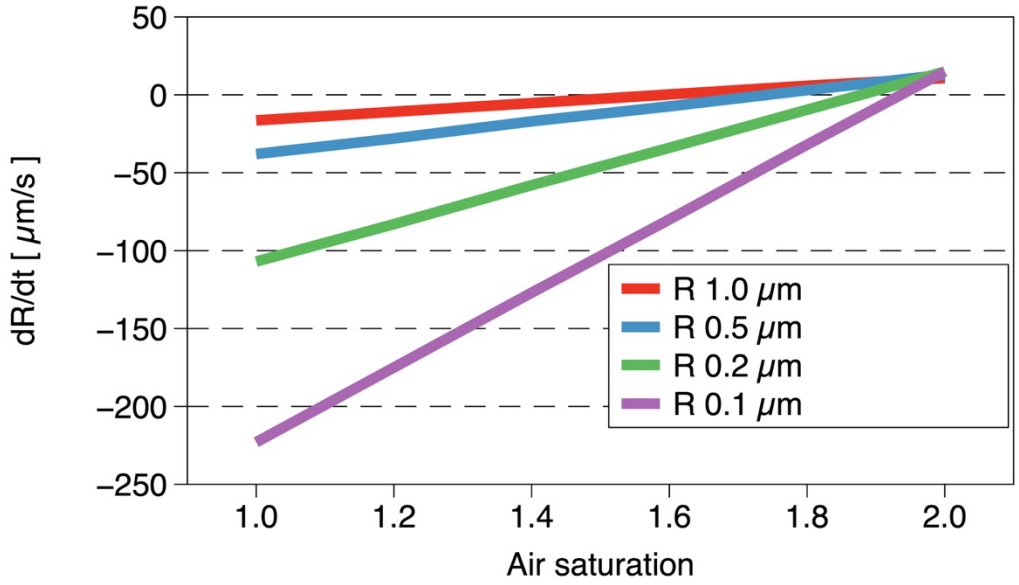

Fig 2. Rate of change in radius (R) due to diffusion for a clean air bubble in water, with a surface tension of 72 N/cm and at 293 K. Calculated from eq (15) in ([77]). A negative value means a shrinking bubble, a positive value means a growing bubble.

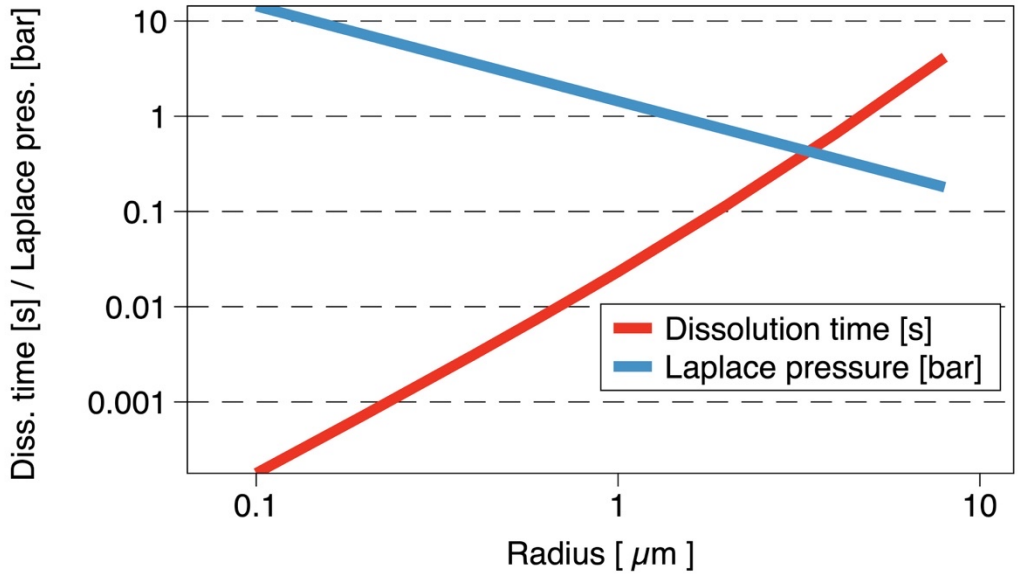

Fig 3. Blue line: Time for complete dissolution of an air bubble in water with 100% air saturation, a surface tension of 72 N/cm and at 293 K. Calculated from eq (17) in ([77]). Orange line: Laplace pressure under the same conditions. Both axes are logarithmic.

Epstein-Plesset made several simplifications in their analysis, and more detailed models have later been developed by others but their predictions have

been experimentally confirmed with rather high accuracy (+-8% for dissolution times)[77]. Epstein-Plesset assumed the bubble to be stationary, i.e. that there is no effect from movement through the liquid. They also neglected any convection resulting from the movement of the interface due to the shrinking of the bubble. They furthermore assumed that the bubble is alone in a large volume, no other bubbles in the vicinity prevents diffusion. And importantly, air was assumed to diffuse freely across a clean air-water interface, with no diffusion barrier at the interface. This last assumption was never clearly stated by Epstein-Plesset, it was just taken for granted. However, this may not always be the case, and this may be of importance for the stability of small bubbles.

3.2 Surface chemistry

From a surface chemical perspective, a micro-/nanobubble dispersion can be seen as colloidal particles as well as a very dilute air-in-water emulsion.

3.2.1 Colloidal stability

A simple, yet useful, model for colloid stability is the DLVO theory, named after its four originators[78]. According to DLVO theory, two colloids are mutually repulsed by electrostatic forces, but attracted by van der Waals forces, and the balance between the two determine the stability of a colloidal dispersion. Van der Waals forces act on shorter distance than electrostatic repulsion and their strength depends on the properties of the colloidal material. The Hamaker constant for a material gives an estimate of the van der Waals force, and is relatively low for organic compounds, compared to many minerals and metals. There are also other material constants related to the van der Waals forces.

Surfaces in water acquire a charge either by ionization of surface groups (e.g. $COOH \rightarrow COO^- + H^+$) or by adsorption of ions from the solution[79]. In either case an electric double layer develops, with an inner, denser, layer of charges and an outer, more diffuse layer of ions of opposite charge. When the colloid moves through the solution, there will be a shear plane in the outer layer, ions outside this plane will not follow the colloid. Experimentally, the effective charge at this shear plane can be measured in the form of a zeta potential [mV], commonly by measuring the speed of colloids induced by an electric field. The zeta potential is strongly affected by pH and by the ionic strength of the solution. Generally, the Zeta potential is negative at high pH and positive at low pH. The isoelectric point, the pH where the zeta potential is neutral,

depends on the colloidal material and can vary widely. An elevated ion concentration will cause the double layer to decrease in thickness and the zeta potential to drop to close to zero. In practice, this is the reason why salt water is generally more clear compared to fresh water in nature. As a rule of thumb, colloidal dispersions with a zeta potential within ±30mV are unstable, whereas higher zeta potentials provide stability. When colloids are stabilized by charge, it is not a direct electrostatic repulsion which prevents colloids from agglomerating. It is rather an osmotic effect, when two colloids approach and the concentration of ions between them increase, water will diffuse into the space to dilute the ions.

In addition to DLVO theory, steric stabilization is an important mechanism. Steric stabilization is due to water soluble polymer chains sticking out from the colloid surface. When two colloids approach, the concentration of polymer chains increases between them and the entropy of the chains decreases. Due to these osmotic and entropic driving forces, water will diffuse into the space between the colloids. Steric stabilization allows colloids to be stable also at high ionic strength.

Hydrophobic attraction can cause rapid agglomeration of particles, and is practically utilized in flotation processes where hydrophobic particles attach to hydrophobic gas bubbles. Hydrophobic attraction on the molecular level is caused by the thermodynamic energy penalty for solvating hydrophobic molecules in water, and is thus caused by the water expelling the hydrophobic molecules rather than the hydrophobic molecules being attracted to each other. Hydrophobic attraction drives for example protein folding and micelle formation, in which cases the molecules are partly hydrophobic and partly hydrophilic. Hydrophobic attraction between larger surfaces and over greater distances is, at least partially, mediated by dissolved gases and nanobubbles, something which is discussed further in chapter 3.7.

3.2.2 Emulsion stability

Emulsion of oil-in-water (o/w) and water-in-oil (w/o) have been extensively studied and are of importance in applications ranging from oil excavation to food and cosmetics. Normally in these applications, the percentage of dispersed phase is high, whereas in the case of nano- and microbubbles (air-in-water emulsions) the volume fraction of dispersed air is low. Emulsions can be either thermodynamically stable (microemulsions) or kinetically stable. In the former case, the emulsion structure is very fine and there is a high concentration of

surfactants. In the latter case there is a thermodynamic driving force for separation, but it takes extremely long time for separation to occur. It seems safe to assume that air-in water emulsions can only be kinetically stable. There are two destabilization mechanisms specific to emulsions, coalescence and Ostwald ripening.

Coalescence is the merging of two droplets into a larger one. Once the droplets have become large enough gravity will separate them by sedimentation or buoyancy. Coalescence is prevented by avoiding the interfaces to get into full contact, e.g. by electrostatic or steric stabilization. Local viscosity is also important in this respect. Once there is a rupture in the film separating the two droplets, coalescence will occur.

Ostwald ripening is due to the Laplace pressure (see chapter 3.1) of e.g. small oil droplets in water. Since the Laplace pressure is higher in smaller droplets, these will have a higher driving force to dissolve, and the larger ones will grow due to the increased supersaturation of oil. This phenomenon require that the oil has a slight solubility in water, which is the case also for air. In the case of submicron air bubbles, the driving force for dissolution is strong, also at lower surface tensions than 72 mN/m.

Whereas o/w and w/o emulsions are most commonly stabilized by surfactants, they can also be stabilized by adsorbed particles through steric hindrance, this is referred to as a Pickering emulsion after one of the pioneers in the field. Particles with 10 -100 times smaller diameter than the emulsion droplets are normally used[78]. The particles need to be partially wetted by both phases. Pickering emulsions can be very stable, when the interfacial tension is high, thanks to the high energy required to remove an adsorbed particle from the interface. With low interfacial tension less energy is required to form the Pickering emulsion, but the particles are also desorbed more easily which results in lower stability[80].

3.2.3 Surface chemistry and bubble stability

As was mentioned in chapter 2.1, surfactant stabilized bubbles – functioning as cavitation nuclei in water – were proposed by Fox and Herzfeld in 1954. They suggested that the main stabilizing effect of adsorbed surfactants would be to slow down diffusion of gas, whereas the decrease in surface tension and thus Laplace pressure would be very moderate.

Later, Yount[40, 81] suggested a model for stable micro- and nanobubbles with a surfactant layer of variable permeability. In this model, the skin of adsorbed surfactants would normally be permeable to gas diffusion, but at rapid compression the skin would become almost impermeable. Furthermore, this model suggests that the surface tension is close to zero due to the very dense packing of surfactant molecules that can be achieved on a curved surface. Yount's experiments did indicate that invisible cavitation nuclei stabilized after a rapid increase of the external pressure, but the evidence is indirect as the nuclei themselves were not detected, only the resulting macroscopic bubbles after decompression. In support of these claims, others have shown that a rapid compression of a monolayer of lung surfactant would stabilize it considerably[82]. It has also been found that in production of phospholipid stabilized contrast agent microbubbles, the freshly formed bubbles shrink 2.5 times in diameter before stabilizing, something which will be further discussed below.

The properties of surfactants are often studied in Langmuir troughs, where a monolayer of surfactant is formed on a plane water surface. The monolayer is gradually compressed by a movable barrier and the pressure required for compression is measured. A poorly water-soluble surfactant will stay at the surface until the monolayer mechanically collapses, whereas a water-soluble surfactant will gently dissolve from the surface as the pressure increases. The surface tension can be determined by subtracting the measured surface pressure from the surface tension of the air/water interface without surfactant (72mN/m). The surface pressure is defined as $\pi = \gamma_0 - \gamma$, where γ_0 is the surface tension of the solution without surfactant and γ the surface tension of the surfactant monolayer.

A surfactant monolayer can exist in different 2-dimensional phases[83, 84], just like 3-dimensional materials can exist in different phases (gas, liquid, solid). When a monolayer of surfactant is compressed in a Langmuir trough, it will transition from one phase to another and this can often be seen as a stepwise jump in surface tension/surface pressure. For historical reasons the phases of a monolayer are usually denoted gas, liquid-expanded, liquid-condensed and solid, although other nomenclatures have also been used. Kaganer and co-workers suggested that the term liquid-condensed be abandoned[84] and only the term condensed should be used for liquid-condensed and solid-condensed. Instead the two condensed phases could be designated tilted-condensed and untilted-condensed, which would more accurately reflect their nature. In the

condensed states the surfactant tails are aligned and organized, whereas in the liquid-expanded state they are more disordered.

The condensed states require that the interface is supersaturated with surfactant molecules[85]. Several phases may coexist in a monolayer, condensed "islands" which float in a "sea" of the liquid-expanded phase may form and gradually expand upon compression until the whole layer is condensed. To reach the lowest possible surface tension, the surfactant layer has to be in a condensed state. Surfactant stabilized microbubbles have been observed to shrink in size by a factor of around 2.5 before stabilizing. This factor corresponds to what is expected for a transition from expanded to condensed state[86].

Common water-soluble surfactants will not reach near zero surface tension on a Langmuir trough, typically not below 20 mN/m. Water insoluble double-tail surfactants, such as phospholipids which constitute a large part of cell membranes and which are used to stabilize contrast agent microbubbles, can however pack very densely on a plane interface and reach close to zero surface tension[87]. Not only can zero surface tension be reached, but even negative surface tension has been suggested for an air bubble under high external pressure[88, 89]. Insoluble single-tail surfactants such as the Spans used in paper II and IV have been reported to reach a condensed state with close to zero surface tension on a Langmuir trough[90]. In the same report, mixtures of insoluble Span and soluble Tween failed to reach such low surface tension, although the same mixtures were shown to generate stable micro-/nanobubbles. However, when the solution had been sonicated to generate bubbles, it had near zero surface tension as measured in the Langmuir trough. Apparently, the sonication caused structural changes in the surfactant dispersion.

It had been suggested that the curvature of small bubbles enables surfactants to pack more densely and reach lower surface tension. However, for bubbles ≥100 nm in diameter, the curvature is not very high compared to the size of the surfactant molecules.

In lipid/surfactant compositions for contrast agents, the water-soluble emulsifier, which typically makes out 10-20% of the composition, have been observed to be squeezed out of the monolayer under compression[91-93]. The interface is then enriched in the less water-soluble components.

Mechanical collapse is observed in Langmuir troughs, and it has also been reported for bubbles stabilized by phospholipids[85] and fluorinated surfactant[94], undergoing shrinkage from 10-20 to 1-2 μm. When reaching 1-2 μm, bubbles appear to be more stable, as they are simply too small for wrinkles to be able to form.

When the surface tension is zero, the shape of a bubble is not necessarily spherical, as there is no internal Laplace pressure that generates a spherical shape. Stable microbubbles which are non-spherical have also been microscopically imaged in several cases[95].

Surface tension close to zero can give bubbles stability in gas oversaturated solutions, but not in undersaturated. The surfactant layer therefore needs to also make out a barrier against gas diffusion. Also, as long as there is any residual surface tension, diffusion prevention is needed for stability. Common water-soluble surfactants and polymers do make out a significant diffusion barrier[96, 97], but do not significantly extend the lifetime of microbubbles in experiments[77].

Borden and Longo examined the permeability of a surfactant layer on a bubble attached to a microscope slide and found an increased resistance to diffusion with the number of carbon atoms in the surfactant tail. The diffusion resistance dependence on chain length was weak up to 18 carbons, above which it increased sharply in the range C18-C24[98]. For condensed monolayers the diffusion resistance has been estimated to 1000 s/cm[99], much higher than for some water soluble surfactants, and the potential lifetime of microbubbles has been estimated to 4000 years based on this fact. Although it has been claimed that the diffusion resistance is insignificant for lipids with 18 or fewer carbons[77], much point in the opposite direction.

An important factor to prevent coalescence is, as mentioned above, surface charge or zeta potential. Since salt limits the zeta potential, it is of little importance for contrast agent microbubbles, which are generally prepared in 1% salt buffer, or for bubbles in sea water. It is nevertheless of potential importance for bubbles in fresh water, and zeta potential measurements for nanobubbles have been reported in several papers[100-105], although many of those papers failed to ascertain that the bubbles were actually bubbles. The reported zeta potentials are often strongly negative, and high negative zeta potential is sometimes even claimed as evidence that detected colloidal particles are bubbles. Negative zeta potential is however common for many types of colloids at neutral or mildly alkaline pH. If a bubble is covered with surfactants, it is the

type of surfactants which determine the zeta potential rather than the bubble itself.

In solutions with high salt concentration, steric hindrance is the most important factor to prevent coalescence. Phospholipid mixtures for contrast agent bubbles therefore normally contain 10-20% of a component with bulky PEG (Polyethylene glycol) chains. This component has been shown to be very important for bubble stability[86]. Additionally, the presence of a high concentration of liposomes (submicron water filled vessels covered with one or several lipid double layers) is also important, as their presence at the bubble surface helps prevent coalescence. Concerning bubbles in natural water, Yount[39] imaged bubbles in a gel with Scanning Electron Microscopy (SEM). After staining the samples with Osmium Tetroxide, which will provide contrast to organic materials, he saw a cloud of organic materials around the bubbles and concluded that a reservoir of surfactants is present and is necessary for stability. These thick layers presumably made out considerable steric hindrance against coalescence as well.

Natural water, including tap water, contains a wide range of organic substances from natural sources[106]. Humic substances (polymeric organic acids) are most notable, often giving fresh water a yellow or brown appearance, but surface-active substances such as fatty acids and carbohydrates are also common. Fatty acids and similar natural surfactants found in water to a large extent has tail lengths of 18 carbons or less[107] and comprise a mixture of saturated and unsaturated chains. Although the composition may not be optimal, it seems likely such substances could stabilize bubbles. The concentration is not very high though. D'Arrigo and co-workers found that extract from forest soil enhanced the number of stable microbubbles they could generate in gel[41, 108-110]. They made a considerable effort to identify the active substances and concluded that lipids with hydrocarbon chains and glycoproteins were the important components. They did however also try many other additives with less success. Johnson & Cooke found when they generated stable micro- and nanobubbles in sea water that large amounts of stable bubbles were only generated in samples taken on some days. Apparently, the amount of bubble stabilizing substances varied. In both the mentioned cases it seem certain that the bubbles were stabilized by surface active substances, and optical and SEM images showed smooth bubble surface and only occasionally an attached particle[39, 95]. It is interesting that considerably higher surfactant concentrations are found necessary for artificial contrast agent bubbles than is present in

natural water. In river or lake water there is often < 10 mg/l organic carbon, in ground water or sea water considerably less. Apparently, there is something left to learn from nature.

3.3 Buoyancy

Once bubbles are stable against diffusion and stable against coalescence, buoyancy/creaming becomes an important factor for stability. The speed of sedimentation of particles and creaming/buoyancy of oil droplets and gas bubbles is expressed by Stokes law[78]:

$$v = \frac{\Delta\rho d^2 g}{18\eta},$$

where $\Delta\rho$ is the density difference between the bubble/particle and the surrounding medium, d is the diameter, g is the gravitational constant and η is the viscosity of the medium. When a particle or bubble is small enough[111, 112], typically well below 1 μm, the Brownian motion will be of the same magnitude as the sedimentation/creaming and the dispersion will be stable. For a bubble, the critical size can be larger if it has heavy material adsorbed. Also, agglomerates of bubbles comprise mostly water and will have a considerably smaller density difference than a single bubble of the same size. As can be seen in the equation, size is however more important than density difference.

3.4 Other theories on bubble stability

3.4.1 Dynamic equilibrium model for bulk nanobubbles

Recently, a dynamic equilibrium model was suggested[113], wherein adsorbed hydrophobic substances are proposed to stabilize bulk nanobubbles. A similar model had previously been suggested for surface nanobubbles[114] (see 3.5). In the present model, the adsorbed substances are completely hydrophobic, without any hydrophilic surfaces. Since gas is attracted to hydrophobic surfaces, it was suggested that a steady inflow of gas is generated at the edges of the hydrophobic material which is balanced by the diffusional outflow of gas from the non-covered parts of the bubble surface, due to Laplace pressure. An important feature of this model is that it predicts that bubbles can be stable not only in oversaturated, but also in slightly undersaturated water (80% saturated). It has been reported that bulk nanobubbles can indeed be generated and survive in mildly gas undersaturated water[115]. The model could potentially also provide an explanation for the many reports of nanobubbles in water with very low

concentration of impurities. The surface coverage needs to be only 50% for stable nanobubbles and much less ($3x10^{-4}$) for bubbles of 2 μm radius. The authors claim the model is valid for rigid material as well as flexible material such as oil. Experimental support for this model is provided by a recent paper[116] where nanobubbles were generated in water with added hydrocarbons or fatty acids. The nanobubble samples were imaged by Transmission Electron Microscopy (TEM) in liquid state in a narrow channel, images show droplets of oil on the surface of apparent air bubbles. The method is not discussed much in the paper, and it could be speculated that bubbles are generated by the electron beam or that solids are misinterpreted as voids. Several other recent papers report enhanced nanobubble generation in dispersions of hydrophobic[117, 118], as well as hydrophilic[119, 120] nanoparticles. The dynamic equilibrium model is discussed in more detail in paper III.

3.4.2 Ionic stabilization

It has been claimed that inorganic ions alone can stabilize nanobubbles, even at concentrations as low as 10^{-6} M[121]. This idea was also treated in a very recent paper[122]. The model suggests that selectively adsorbed anions create a coulombic repulsion, which counteracts the pressure from the surface tension. This idea has been questioned based on; 1) The charges when compressed should diffuse in to the liquid rather than stay at the surface and generate a pressure along the interface[123], 2) The pressure from the ions has been calculated to be negligible compared to the other forces at work[72]. Other authors have also claimed that addition of salt helps stabilizing nanobubbles[103] and based on this, it has become popular among researchers to add NaCl to water when performing nanobubble experiments. One possible explanation why inorganic salts may benefit nanobubble stability is that salts will decrease the solubility of surfactants, also known as the salting-out effect. As mentioned above, bubbles can be stabilized by poorly soluble surfactants, and salt may push slightly soluble surfactants to become insoluble. Salt may also affect the repulsion between bubbles and thus the probability of coalescence. Higher salt concentrations will shield surface charges and decrease the zeta-potential, which can increase coalescence. This has also been found experimentally[103, 104] for bubbles. Salt can also enhance agglomeration of particles and oil droplets which may be mistaken for bubbles.

3.4.3 Water structure

Based on ATR-IR measurements[124, 125] and Raman measurements[126] on nanobubbles in distilled or deionised water, it has also been suggested that a specific water structure at the air-water interface prevents gas diffusion or counteracts the Laplace pressure[127,110].

3.5 Surface nanobubbles

Nanobubbles on surfaces have been experimentally and theoretically investigated in many papers[128, 129] and is a less controversial entity than bulk nanobubbles. Atomic Force Microscopy (AFM) is the main method to detect and study surface nanobubbles, but also other methods have been utilised, such as Quartz crystal microbalance (QCM), Surface Plasmon resonance (SPR), Fluorescence microscopy, Small-Angle X-ray scattering (SAXS) and liquid TEM. It has been reported that silicon oil droplets emanating from commonly used plastic syringes can form droplets on surfaces which can be mistaken for surface nanobubbles[130, 131]. This is important to keep in mind when studying the literature, especially concerning older papers in the field. Recently, contamination from syringes was also reported to generate stripe patterns on surfaces[132], as measured by AFM.

Since dissolved gas has an affinity for hydrophobic surfaces, formation of nanobubbles occurs much more readily on such surfaces, although they have been observed also on hydrophilic surfaces. Several mechanisms have been proposed and the one that appear most accepted[129, 133] stresses the importance of pinning of the contact line of the bubble. Pinning requires that the surface is not perfectly smooth. The pinning has also been shown to be destroyed by addition of surfactants. If the contact line is pinned, the curvature will decrease as the bubble shrinks due to the Laplace pressure, the Laplace pressure will thus decrease as the bubble is getting smaller, contrary to what is the case for a spherical bubble in the bulk or a surface bubble without pinned contact line. The pinning stabilization model states that the driving force for diffusion from the bubble due to Laplace pressure is balanced by the driving force for the bubble to grow due to gas oversaturation and that this balance is achieved at a certain contact angle. The contact angle is thus dependent on the degree of oversaturation. The model matches experimental findings of generally low contact angles and that irregularities on the surface are beneficial for stable bubbles to form.

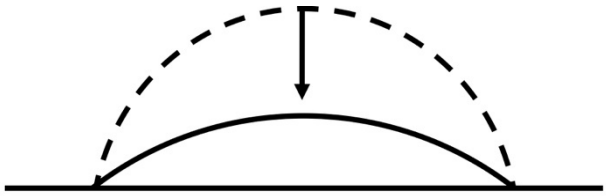

Fig. 4. Shrinking surface nanobubble with pinned contact line.

The above model states that surface nanobubbles can only be stable in oversaturated water. Very recently, a modification of this theory was proposed[134, 135], where the affinity of gas to hydrophobic surfaces was also taken into account, predicting stable surface nanobubbles to be possible also in slightly undersaturated water. This model also states that oversaturation and hydrophobicity are not simultaneously necessary, only one of these criteria is necessary for surface bubble stabilization. This model also matches experimental findings that bubbles are stable over long time in open systems and react remarkably slowly to degasification. It also matches experimental observations of bubbles on hydrophilic surfaces. This paper by Tan et al effectively reintroduces the previously abandoned dynamic equilibrium model[114], but combines it with the contact line pinning model. Meanwhile, some researchers claim that surface nanobubbles contain gas of an exceptionally high density[136, 137], but this does not appear to be generally accepted.

3.6 Nanobubbles on particles and in crevices

Early on in cavitation research, cavitation nuclei were suggested to consist of solid particles with air pockets in cracks and crevices[18, 138], these are sometime referred to as “Harvey nuclei” after the original author. More recent research has confirmed that particles can act as cavitation nuclei[26, 27, 139-141] and that after several cavitation events the particles ability to nucleate bubbles is exhausted, evidencing that air bubbles on the particles are the actual nuclei. A certain regeneration is however taking place under repeated cavitation[28]. Different particles have a widely varying ability to nucleate cavitation and this seems to be related to surface structure[26], size[139] and hydrophobicity[27]. A rough surface structure is more important than deep pores, which would suggest that bubbles are located on the particle surface rather than in cracks and pores, and are pinning-stabilized similarly as bubbles on a flat surface. Smooth larger particles (76μm) were shown to be more active nuclei than smooth small ones (3μm), also indicating surface bubbles. What also speaks against the crack/crevice

model is that bubbles in cracks and pores are very small, whereas they need to be of a minimum critical size in order to nucleate cavitation[140]. The crevice model has however been confirmed by cavitation experiments with etched 100-1000 nm wide cylindrical pits on a flat hydrophobized silica surface. Cavitation could be nucleated only once per pit[142]. The experiments fitted well with the theoretically expected relation[143] between pit size and the pressure amplitude necessary to generate cavitation. For cylindrical pits of 50-60 nm diameter, the required pressure pulse amplitude is very high, 20-30 bar. For more moderate pressure amplitudes, larger pits are required for nucleation. Thus, the crevice theory holds well for cavitation at macroscopic surfaces – where indeed cavitation is more commonly observed than in the bulk of the liquid.

In recent years the crevice model has inspired the development of a new type of ultrasound contrast agent, where cavitation bubbles are generated in situ on particles[144]. One such particle type, cup-shaped polymer particles with a cavity diameter in the range 100-700 nm, were reported to cavitate in accordance with theory, with the largest cavities having the lowest cavitation threshold (about 10 bar). Another interesting example is hydrophobized 300nm silica particles with a lipid coating to prevent agglomeration due to hydrophobicity. This particle type would only act as nuclei when the lipid coating is in a condensed state, which is believed to be because bubbles nucleate in the cracks of the coating, exposing the hydrophobic particle surface. It is interesting that cavitation here is taking place from a very small nuclei, although it is plausible that there is also a certain gas accumulation under the lipid coating, due to the hydrophobic effect.

Water need to be filtered at 1 μm or less to increase its resistance to cavitation according to some reports, whereas others report a gradually lowered cavitation threshold from 20 to 5 μm filtration[145]. Such filtration experiments do not even tell us if particles or microbubbles are active as nuclei, even less about the nature of present particles. Based on the latest research, it seems likely that irregular particles or particle agglomerates several μm large can host crevice bubbles a few hundred nm in diameter. To what extent they can stay sufficiently hydrophobic in water is however an outstanding question, as hydrophobic surfaces can be expected to become coated with surface active substances.

3.7 Nanobubbles and the hydrophobic attraction

Attraction between hydrophobic molecules or parts of molecules is a well-known and important phenomenon, but from the early 1980s[146] and onwards

there were also numerous reports of a long-range attraction between hydrophobic surfaces. This force seemed to have two different regimes, a longer range from 25nm to 100nm or more, and a shorter range from 10-25 nm. The research conducted on the long-range hydrophobic attraction was actually what eventually led to the discovery of surface nanobubbles. The long-range hydrophobic force turned out to be not an actual force, but due to bridging of pre-existing nanobubbles on the hydrophobic surfaces[15, 147]. This explained why the effect was poorly reproducible. It was shown that the attraction decreased to varying degree if the water was degassed. Furthermore, studies using AFM have shown a repulsive force preceding an attractive jump. The initial repulsion was shown to be pH dependent, which indicates that it is due to electrostatic repulsion between charged bubble surfaces.

Interestingly, the long-range hydrophobic attraction has in one paper been shown to be influenced by neutron radiation[34]. This further confirms the bubble generating effect of neutron radiation, mentioned in chapter 2.1. Neutron irradiation of the solution prior to injection in the sample cell enhanced the magnitude and distance of the attractive force. This could mean that bubbles generated in the bulk of the solution by neutron irradiation adsorb to the surface and enhance the long-range hydrophobic attraction.

The shorter-range hydrophobic attraction at decay lengths of less than 25 nm is more mysterious and believed to have other causes. Degassing was shown not to affect the short-range attraction[148]. A recent (2016) review states that evidence for short-range hydrophobic attraction in the range 5 – 25nm is scarce[149]. After 30 years of research there is only two papers that show such an effect unambiguously, according to this review.

Very recent work does however provide further evidence of a hydrophobic attraction force in this range[150-153]. Ishida and co-workers showed the force to increase monotonously with increasing hydrophobicity (measured contact angle) of the surface. They cautiously suggest that cavitation between the surfaces is responsible, thus gas would be involved also in this case. Schlesinger showed the force to be diminished by degassing and went on to provide evidence of a thin layer of adsorbed gas molecules at a hydrophobic surface. Two other recent studies also report thin gas layers on surfaces[154, 155].

Practically, Pashley showed[156] that oil could be stably emulsified in water without addition of any surfactant if the water was degassed very thoroughly beforehand. The degassing took place by repeatedly freezing and thawing the

water under vacuum, a well-known method to reach very low concentration of dissolved air. By removing the air, the attraction between the hydrophobic oil droplets decreased since no bridging bubbles were present to help them agglomerate and coalesce. Pashley later went on to demonstrate an enhanced cleaning ability of such degassed water[157].

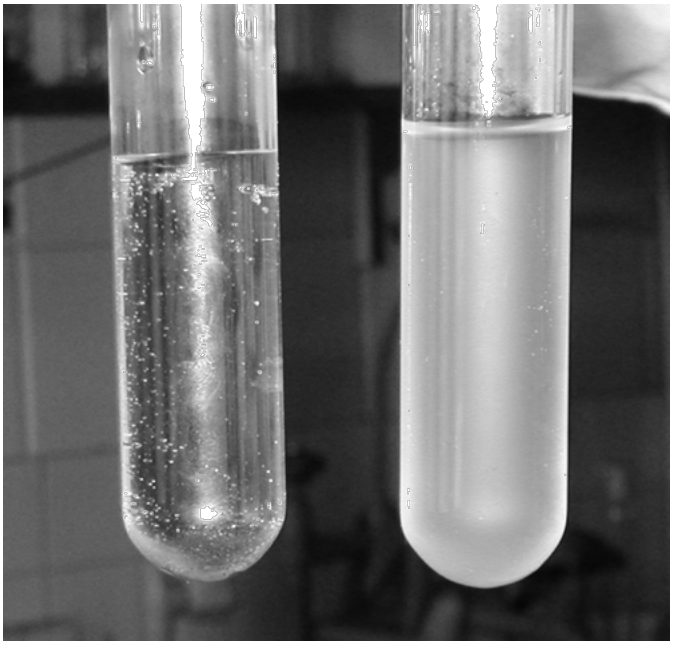

Fig. 5. Photograph of gassed (left-hand side) and de-gassed (right-hand side) water shaken vigorously with oil (perfluorohexane). Reprinted with permission from R. M. Pashley, M. Rzechowicz, L. R. Pashley, M. J. Francis, De-Gassed Water Is a Better Cleaning Agent, J. Phys. Chem. B 109 (2005) 1231-1238. Copyright (2005) American Chemical Society.

3.8 Bubbles under pressure

Destruction of bubbles by pressure treatment can be used to differentiate bubbles from other light scattering particles and droplets. There are many reports on destruction of micro- and nanobubbles by pressurization, although some of them are indirect evidence in cavitation experiments where the character of the "cavitation nuclei" is unknown. Some of these reports were mentioned in chapters 2.1 and 2.2. It is not entirely obvious how bubbles are destroyed by pressurization as several mechanisms are possible. Johnson and Cooke[95] observed bubbles in the size range 0.5-10 μm in an optical microscope. The bubbles were generated in sea water and stabilized by adsorbed impurities. Upon a pressure rise by only 0.083 bar, many, but not all, bubbles rapidly dissolved. Smaller bubbles were to a greater extent unaffected. A pressure increment by 0.14 bar removed all visible bubbles. These bubbles were apparently less resistant to pressure than in many other reports. More recently

the number of nanobubbles, as measured by a particle counter, were shown to be reduced after exposure to 2.4 bar pressure[158] and as measured by NTA to be reduced after 500 bar[159]. These nanobubbles were generated in more or less pure water and any stabilizing contamination is unknown. The average size increased after pressurization with the maximum effect achieved after 10 minutes. The number reduction and size increase appeared to be somewhat lower after 60 minutes pressurization than after 10 minutes.

Monolayers of surfactants are well known to wrinkle and fold under pressure on a flat surface in a Langmuir trough as well as on a microbubble shrinking by diffusion[94, 98]. When a microbubble after several wrinkling-induced collapses reaches a size of 1-2 μm, it appears to be considerably more resistant to further wrinkling. It seems likely that at some size a bubble will be too small to have room for any wrinkles. Thus, a large lipid-coated microbubble can be expected to undergo wrinkling induced collapse under moderate external pressure, but a smaller one will be considerably more resistant to collapse. Smaller lipid-coated bubbles will instead experience a compression of the lipid monolayer. In a recent paper[88], about 1 μm large lipid-coated C_3F_8 bubbles were measured by DLS while the pressure was increased from 1 to 5 bar. The bubbles were seen to decrease in size upon compression and increase in size again following decompression. The size increase after decompression was however only temporary, within minutes the size decreased back to similar magnitude as under compression. It appears that in this case the bubbles were destroyed during the decompression rather than during compression. It is possible that if the lipid monolayer was damaged after decompression, and the liquid was oversaturated with gas, some of the bubbles grew and acquired buoyancy and disappeared from the solution. This can be seen as a cavitation event. The authors furthermore concluded that the surface tension became negative during compression, which made the bubbles to some extent resist compression. They estimated the surface tension to -15 mN/m, and the Laplace pressure to -0.8 bar. This means that there is a sub-pressure in the compressed bubble, which implies that when the lipid shell opens up during decompression, more gas will diffuse into the bubble.

Yount on the other hand, studying “cavitation nuclei” in the range 0.1-1.0 μm in agarose gel, considered the speed of compression more significant than the total pressure magnitude for destruction of nuclei[38]. A stepwise compression was shown to destroy fewer nuclei than a single pressure increment of the same total magnitude.

It should also be considered that an increase in pressure of several bar can take the liquid from a state of supersaturation or saturation, to a state of considerable undersaturation according to Henry's law. This can provide a considerable driving force for diffusion from the bubble and thus dissolution. A negative Laplace pressure, as reported by Alheshibri, can to some extent balance this driving force for dissolution, but not fully cancel it. If there is air/gas available on top of the liquid, it will eventually diffuse into the liquid and cause saturation at the elevated pressure. Decompression will then yield a considerable oversaturation which can generate cavitation/macroscopic bubbles or micro/nanobubbles. Generation of macroscopic bubbles will deplete cavitation nuclei, i.e. nanobubbles, but there are also reports of generation of nanobubbles following pressurization and slow decompression[115]. Macroscopic bubble formation is encouraged by rapid decompression which is well known in the case of decompression sickness.

The issue of diffusion and oversaturation complicates matters and suggests that for destruction of nanobubbles, short pressurization times and rapid decompression is most suitable. In water which is free from stirring and convection, the rate of change of the concentration of dissolved gas is governed by diffusion, which is described by Fick's 1st and 2nd law. If there is no movement in a liquid, it takes very long time to equilibrate with air, on the scale of hours and days[160]. However, when there is a large driving force, such as under pressure, the speed of diffusion increases considerably.

3.9 Bubbles under vacuum

In addition to elevated pressure, vacuum can also be used for destruction of bubbles and thus to differentiate bubbles from other light scattering particles and droplets. Johnson and Cooke, who also observed bubbles under pressure, observed bubbles in sea water in the size range 0.5-10 μm in an optical microscope at mild subpressure[95]. The bubbles expanded under sufficient subpressure and most bubbles returned to their previous size when the pressure was returned to normal. Some did however proceed to shrink and disappear following this vacuum treatment. Overton[161] observed an increased resistance to cavitation for several different water qualities following degassing by heating under strong vacuum (2.7mbar), which was interpreted as due to destruction of gaseous cavitation nuclei. In recent years some authors have used various vacuum treatments to degas the solvent prior to bubble generation to prove the bubble nature of light scattering objects[115, 162, 163]. Others have

vacuum treated probable bubbles in solutions, with varying results[119, 164-166]. Zhou and coworkers found that microbubbles disappeared after 1h at 0.05 bar, but not nanobubbles. Addition of degassed water to a bubble solution has also been used[167] as a means of destroying bubbles by causing air undersaturation. Vacuum degassing has also been applied to surface nanobubbles[115, 168, 169]. Fang and coworkers recently generated both surface and bulk nanobubbles by applying mild vacuum (0.5 and 0.1 bar respectively) for short time. Surface nanobubbles were generated after 5 min vacuum, but disappeared again after 20 min vacuum. Bulk nanobubbles increased in number for 20 min, but disappeared after longer time under vacuum. In both cases much fewer bubbles were generated if the water had been degassed by freeze-thawing at 0.1 bar. To conclude, nano- and microbubbles can increase in size[95] or be generated by mild vacuum[115] for short time. After longer time under vacuum they will however be destroyed due to high undersaturation of gas. To destroy bubbles by causing undersaturation under vacuum, long time and either small distance for the air to diffuse from the bulk of the liquid to the surface, or stirring or convection is beneficial.

3.10 Review of bubble detection methods

Many methods have been suggested and demonstrated for identification of small light scattering objects as actual nanobubbles. Pressure and vacuum/sub-saturation are treated in chapter 3.8 and 3.9. Holography and phase microscopy are treated in chapter 4.4. Below is a brief review of other methods.

Cryo- SEM/TEM

Water, rapidly frozen in liquid nitrogen or helium, is sliced and imaged in a scanning electron microscope or transmission electron microscope. The method has been used in several cases for nanobubbles[124, 170-172], which are visible as voids in the ice. The method has merit as submicron voids do not appear to be a general feature of frozen water. Artefact bubbles generated during freezing has however been reported[173], and it has been claimed that the electron beam may generate bubbles in cryo-samples[174]. One way of avoiding electron beam damage is to cast a thin-film replica of the ice surface, and image the replica in SEM. This method has been used for nanobubbles in some of the mentioned references above. Imaging of nanobubbles in a gel or polymer matrix, is another alternative which has been demonstrated in the past[39].

Liquid-cell TEM

Imaging of liquid samples confined in a very narrow channel in a transmission electron microscope. The method has been demonstrated for nanobubbles[116, 175]. This is a very powerful method as it allows imaging of very small colloids in their native dispersion. However, bubble generation by the electron beam has been reported[176, 177], as well as due to electron beam damage to the sample cell[178], which makes it possible to get false positive results for bubbles.

Fluorescence microscopy

The fluorescence lifetime of Rhodamine 6G is different at air-water interface than elsewhere, this has been used to identify surface nanobubbles[179]. The method appears to not have been tested for nano- or microbubbles in bulk.

Vibrational Spectroscopy

FTIR/ATR has been used to detect gaseous CO_2 in nanobubbles, since the signal is different from that of dissolved CO_2[164, 180, 181].

Oxygen concentration

By adding oxygen-filled nanobubbles to N_2-purged solution and measuring the oxygen concentration over time, the bubbles were showed to release oxygen[182]. Oxygen concentration measurement has also been used to measure the amount of oxygen bubbles attached to particles for environmental remediation[70]. Winkler titration has been used to detect oxygen nanobubbles produced by electrolysis[183].

Cavitation / ultrasound response

For contrast agent bubbles this is, naturally, a common method. Gas bubbles resonate and respond many orders of magnitude stronger to ultrasound than solid particles, this is why they are used for contrast in ultrasound imaging. Ultrasound can be used to detect stable resonance of bubbles, as well as to induce cavitation from a smaller gas nuclei. Ultrasound response is however less used in other bubble research, but could have further potential to detect stable bubbles in liquid. Detecting bubbles as small as 100 nm in limited concentrations may however be challenging.

Centrifugation

Centrifugation can carefully separate particles/bubbles of different buoyancy, and thus separate bubbles from particles. It has been demonstrated in combination with integrated light scattering, to search for nanobubbles[184]. Centrifugation is a common method in the contrast agent field to separate different size fractions of bubbles.

Resonant Mass measurement (RMM)

This method measures the weight of individual particles in a narrow microfluidic channel. It can differentiate between particles of negative and positive buoyancy and therefore potentially differentiate between bubbles and particles. However, oil droplets often have a density lower than water and can thus be mistaken for bubbles. By dispersing suspected bubbles in water of different density (D_2O/H_2O mixtures), their density can be determined. This has been used to identify suspected bubbles as probable oil droplets[185] since their density was only slightly lower than that of water. However, clusters of bubbles could also have a density only slightly lower than 1 g/cm^3 since clusters contain mostly water.

4 Experimental methods

4.1 Theoretical base of experimental methods

4.1.1 Light scattering theory

Measurement methods based on light scattering are the most commonly used for determining the size and concentration of particles, bubbles and droplets in water. Bubbles, particles and oil droplets, etc, hereinafter named "particles" for simplicity, will always scatter light. Even individual molecules scatter light, giving rise to a measurable background scattering signal from pure solvents.

How particles scatter light depends very much on their size, and different laws govern different size ranges. Very large particles behave rather similarly to any macroscopic surface. They will scatter light of different wavelengths similarly. Very small particles, with a diameter less than 1/10 of the wavelength of the incident light, exhibit Rayleigh light scattering. In this size range, the scattering intensity is the same in the forward and backward direction. The scattering intensity at 90° is half of that in the forward and backward direction.

The intensity of scattered light from a spherical particle in the Rayleigh region is given by[186]:

$$I_S = \frac{8\pi^4 N R^6}{\lambda^4 r^2} \left| \frac{m^2 - 1}{m^2 + 2} \right|^2 (1 + cos^2\theta) I_i$$

Where θ is the scattering angle, N is the refractive index of the medium, $m = n_1/n_2$ the ratio between the refractive index of the particle and the medium, R is the radius of the particle, λ is the wavelength, r is the distance from the particle to the point of observation, and I_i is the intensity of incident light. The equation assumes that the incident light is unpolarized.

As can be seen, the scattering intensity is strongly dependent on the particle size (~R^6). It is also strongly dependent on the wavelength (~λ^{-4}), a particle will scatter blue light 6 times more than red light. In an everyday context, Rayleigh scattering is very visible. The blue colour of the sky is due to blue light being scattered by air molecules in the atmosphere.

When the particle diameter is 1/10 to 1/1 of the wavelength, the particles are said to exhibit Mie scattering. Mie theory is however also used to describe scattering also for considerably larger particles, up to tens of μm in diameter.

The Mie theory is essentially a solution to Maxwell's equations for scattering of a sphere. It is rather complex and custom software is used for calculations, as a single formula is not enough to describe it. In the Mie scattering range, the scattering intensity is not monotonically increasing with particle size due to resonance effects, and the size dependence and wavelength dependence is considerably weaker than in the Rayleigh region. Forward scattering is stronger than backward scattering. As the scattering intensity for small particles is higher for shorter wavelengths, green and blue lasers are most commonly used in modern light scattering measurement equipment.

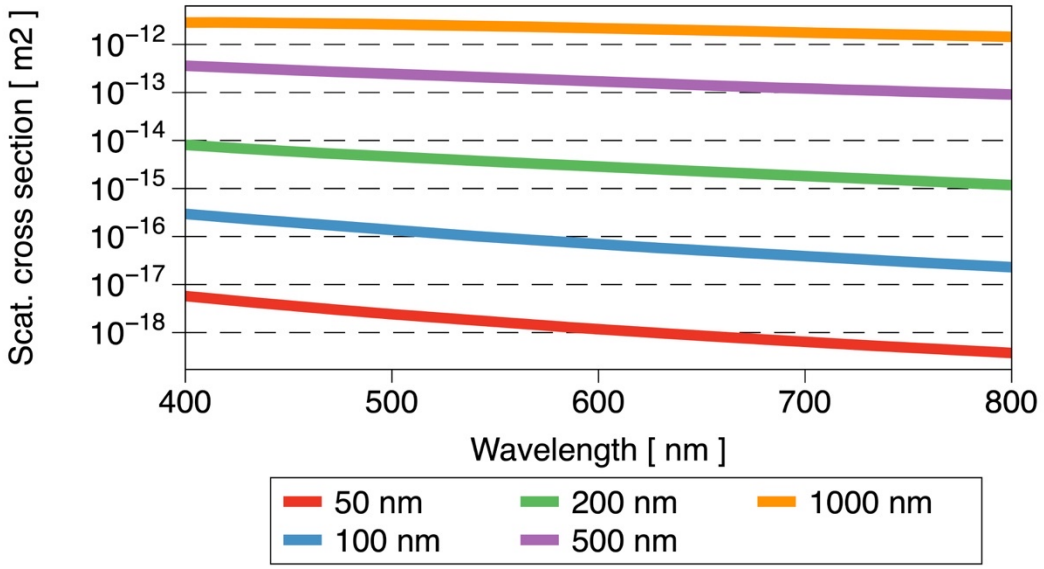

Fig. 6. Calculated Scattering cross section vs wavelength for Polystyrene Latex Particles of different sizes.

Light scattering intensity is also dependent on the difference in refractive index between a particle and the surrounding medium. This is valid also if the refractive index of the particle is lower than the medium, as is the case for gas bubbles in water or other liquids. The refractive index difference for a gas bubble in water is 1.00 (air) – 1.33 (water) = – 0.33. For comparison, the difference for Polystyrene latex particles is 1.59 – 1.33 = 0.26. A single clean air bubble can thus be expected to scatter light more strongly than a PSL particle, which is already a comparably strong scatterer. Other commonly measured particles such as silica (1.44), biological cells, proteins and extracellular vesicles, are considerably weaker light scatterers.

4.1.2 Brownian motion

Very small particles in a liquid or in a gas will move randomly due to their non-uniform collisions with the surrounding molecules, this movement is referred to as Brownian motion after botanist Robert Brown, who studied the phenomena extensively in microscope[187] for pollen particles dispersed in water. However, random motion of dust particles in air had been observed already two millennia earlier, and already then been speculated to be due to collisions with smaller particles and atoms[188]. Albert Einstein published a landmark paper in 1905, theoretically explaining how random collisions between a particle and the molecules or atoms of the surrounding medium would occasionally be non-uniform for sufficiently small particles, causing the particle to move in random directions. Fig. 7. shows this in a conceptual way, however in reality the number of simultaneous collisions is much larger and the non-uniformity smaller. The average kinetic energy of the molecules in the medium is proportional to temperature, T (K) and Boltzmann's constant, k_B (J/K). The higher the kinetic energy of the molecules in the medium, the more vigorous the Brownian motion will be. Furthermore, smaller particle size and lower viscosity of the medium will allow more movement. The diffusivity or diffusion coefficient of a freely diffusing particle in the bulk can be seen as a measure of its positional fluctuation[187] and is related to the particle and the medium properties as:

$$D = \frac{k_B T}{6\pi\eta R},$$

where η is the viscosity of the liquid and R the hydrodynamic particle radius. This formula is referred to as the Stokes-Einstein relation. Note that this is valid for spherical particles, if this relation is used to determine the size of non-spherical particles an error will be introduced. Interestingly, the diffusivity is independent of the mass of the particle. Strictly, the mass does have an influence, but the inertia can be neglected on the time scales normally probed when analysing Brownian motion.

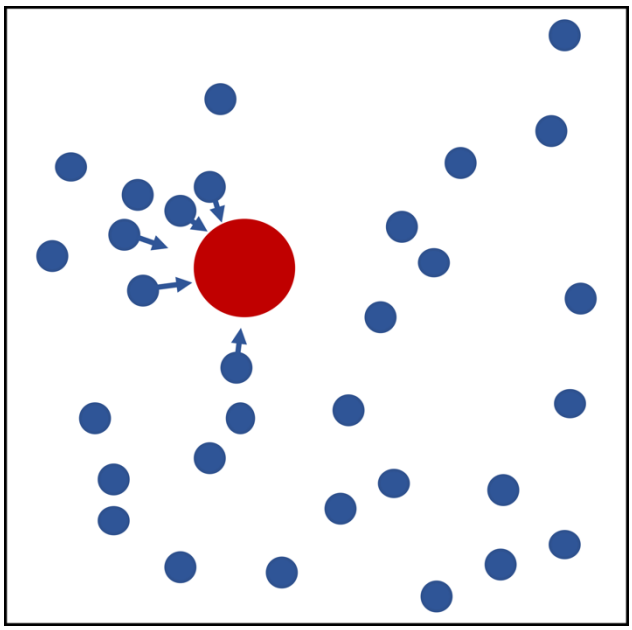

Fig. 7. Conceptual image of an inhomogeneous distribution of molecules (blue dots) bouncing against a particle (red), which will cause it to move.

4.2 Dynamic light scattering (DLS)

Dynamic Light Scattering (DLS), also known as Photon Correlation Spectroscopy (PCS) is a rather mature technology. It has been used since the 70'ies and had its great commercial breakthrough in the 1990'ies. Its' progress has benefitted greatly from the rapid increase in computational capacity available. A liquid sample is illuminated by a laser and a detector is placed at a certain angle in relation to the laser beam. The detector is highly sensitive, it is essentially counting individual photons. Due to interference between light scattered by different particles, a speckle pattern will be generated in the scattered light. Due to the Brownian motion of the particles, this speckle pattern will exhibit fast fluctuations. Over a larger area these fluctuations will average out, therefore the detector measures the photon count rate or scattering intensity for a very small area[189].

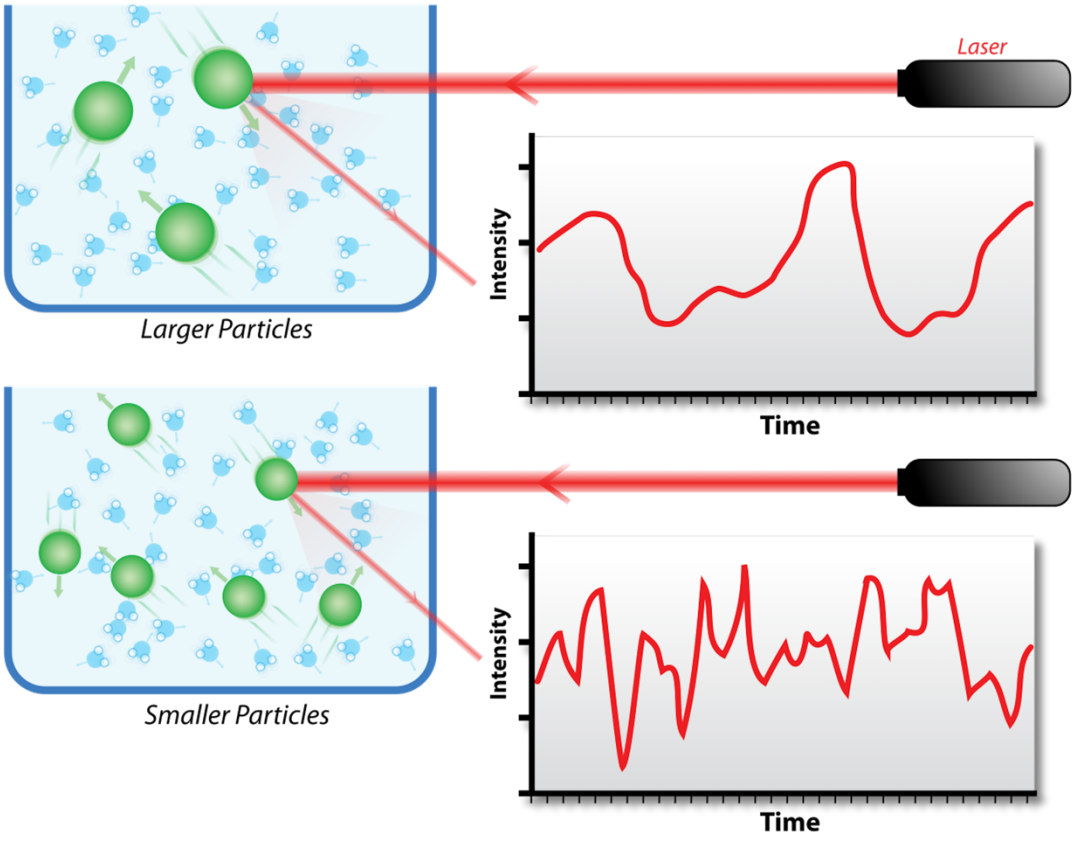

Fig 8. Fluctuations in scattering intensity from large and small particles. Image by Mike Jones, original work for Wikipedia, distributed under a CC-BY 2.0 license.

This time-varying signal can be translated into a correlation function, where the scattering intensity at an arbitrary time (t) is correlated with the scattering intensity after a time increment Δt. Thus, the correlation between the scattering intensity at time (t) and time (t+Δt) is calculated for a wide range of Δt. A plot of the normalized correlation function versus Δt will show a decay from a value close to one at small Δt, to zero at large Δt. The Δt at which the correlation function decays will be correlated to the particle size.

For a monodisperse sample of spherical particles, the correlation function will be proportional to $e^{-Dq2\Delta t}$, where q is the scattering vector and D is the diffusion coefficient of the particles. From this, D can be calculated, and with knowledge of the viscosity of the liquid and the temperature, the particle radius can be calculated from the Stokes-Einstein equation.

For a polydisperse sample, the decay will be more stretched out. There are several mathematical methods which deals with such data to interpret the correlation function into a distribution of sizes. But as DLS is a statistical

method based on the mixed scattering signal from a large number of particles simultaneously, it has limited ability to determine in detail a distribution of different particle sizes. As a rule of thumb, DLS cannot distinguish a mixture of two different size populations where the size of the larger particles is less than three times the size of the smaller particles. Thus, a mixture of monodisperse 50nm and 100nm particles will look like one single population with sizes in the entire range, and an average particle size somewhere in between 50 and 100nm.

Small particles in the Rayleigh scattering region will scatter with equal intensity in the forward and backward direction, whereas with increasing size the forward scatter will be relatively stronger than the backscatter. This can be utilised by selecting a scattering angle where the particles of interest give the best signal. For small particles, interference from larger particles can be avoided by measuring at high scattering angles. For large particles a stronger signal, if desirable, can be achieved at low scattering angles.

DLS can be used over a large size interval, from molecules of single nm size to several μm. The concentration range is strongly dependent on the particle size. The upper concentration limit is limited by the sensitivity of the detectors which can be destroyed by strong light scattering, as well as by multiple scattering which can seriously skew the results. Multiple scattering is when scattered light by one particle is scattered a second time by a second particle.

4.2.2 DLS instrument - ALV-CGS-8F

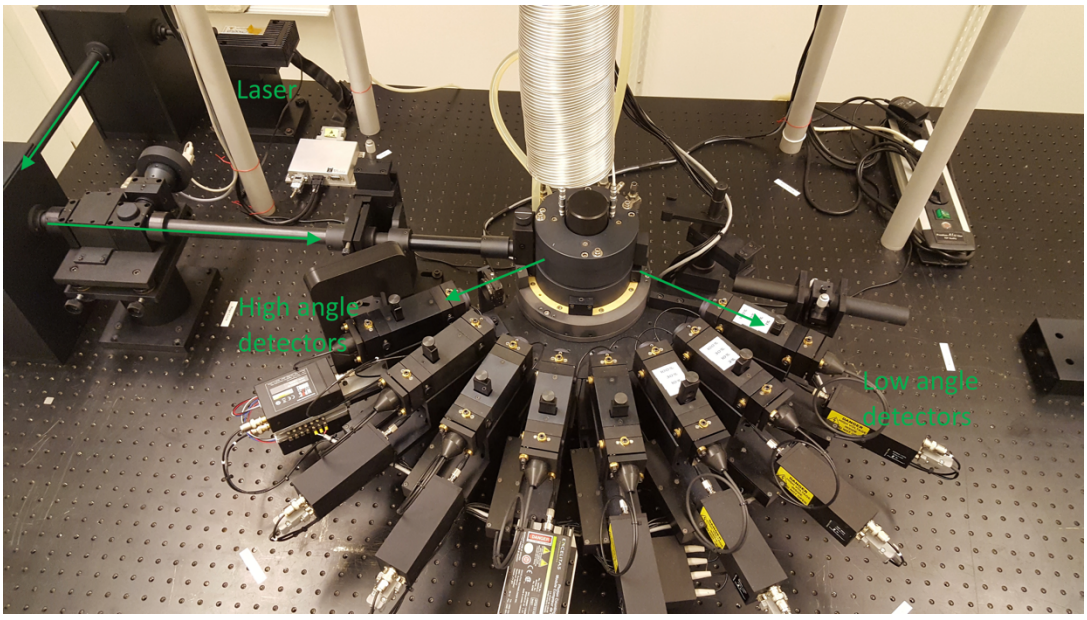

Fig. 9. ALV-5000

The customized ALV-5000 is a research-type instrument with 8 detectors. The light generated by the laser (Oxxius 532S-50-COL-OE, 532 nm, 50 mW output power), passes two mirrors, followed by an automatic attenuator which can adjust the power of the beam that reaches the sample. This feature is to protect the detectors from too intense light which can destroy them. The laser beam then impinges on a cylindrical 8mm cuvette containing the liquid sample. The cuvette is placed in a cylindrical glass container filled with toluene. Toluene has a similar refractive index as the glass, which limits spurious scattering from the wall of the cuvette. This feature is primarily important for static light scattering, where the angle dependence of the scattered light is analyzed, whereas for DLS it is of less importance. The side of the vat is visible from the detector side. The detectors are mounted 17° apart and the entire set of detectors can be moved to cover a wide range of scattering angles. The detectors are PM-tubes from Perkin-Elmer (MP963). The detected optical signals are treated by two correlators (ALV-7004) who handle 4 detectors each and have a capacity of 7.68 billion correlations per second. The measurement and correlation data is collected and visualized by a PC software, which generates a correlation function plot, an intensity plot over time, and an error residual plot and finally a table over the averaged scattering intensities for each detector. A post-processing for each measurement can be made to calculate the particle size distribution.

4.3 Nanoparticle Tracking Analysis (NTA)

This technique is younger than DLS, the first commercial instruments were introduced in the 00's, and has quickly gained popularity. Compared to DLS, it can measure at somewhat lower particle concentrations and better resolve hetero-disperse samples since it is detecting individual particles. It can also directly measure the particle concentration, as each individual particle in the illuminated sample volume is counted. NTA is most generally used to determine the size of light scattering particles, but it is also commonly used to determine size of fluorescent particles and to determine the zeta potential of particles and surfaces.

The equipment is simple and robust, essentially consisting of an optical darkfield microscope, equipped with a digital video camera, a laser and a sample cell. The liquid sample is illuminated at 90° angle to the line of view, which causes light scattering particles to appear as bright spots on a black background. The scattering intensity of an individual particle is strongly

dependent on size (~R^6) in the Rayleigh scattering regime and a function of the refractive index difference between the particle and the liquid. For particles with moderately high refractive index the detection limit is about 30 - 35 nm, whereas certain types of metallic particles can be detected down to 10 - 15 nm due to plasmonic resonance effects. The upper size limit is due to that larger particles undergo less detectable Brownian motion, as well as more sedimentation/flotation, and is about 1000 - 2000 nm.

A video file is recorded during typically 30 - 60 s and is subsequently processed to identify the particles in view and determine their position in two dimensions (x,y) in each image. By comparing the different positions at different points in time, the mean square displacement (MSD) is estimated. This can in be done in different ways, the most common is the following[190]:

$$MSD = \frac{1}{N-n}\sum_{i=1}^{N-n}(r_i - r_{i+n})^2, \quad n = 1, 2, \dots, N-1$$

, where N is the number of frames, r_i is the position in frame i, and r_{i+n} the position n frames later. From the mean square displacement (MSD), the diffusivity (D) can be determined according to[191]:

$$D = \frac{MSD}{2dt}$$

, where t = time, and d is the dimension. For MSD in one dimension, d=1, two dimensions, d=2, and three dimensions, d=3. NTA is normally performed in only one or two dimensions, since the vertical position is difficult to determine. From the diffusivity, the particle size can be determined with the help of the Stokes-Einstein relation.

The particle concentration of the sample needs to be low enough for individual particles to be visible in the image and tracked without interference from neighbouring particles. The upper concentration limit is instrument specific, but commonly about 10^{10} particles per cm^3. More concentrated samples will need to be diluted. On the lower side, a sufficient number of particles need to be visible and tracked to get a statistically reliable result. If very few particles are visible in the field of view, a flow can be applied while the film is recorded. This allows a larger number of particles to be tracked within a certain time frame. The lower concentration limit for such measurements is about 10^6 particles per cm^3. Since the illuminated volume in the field of view is known, the number concentration of particles can be directly determined with this method. Since every single particle is tracked and size determined, a detailed

size distribution can be generated. This allows for several separate particle populations in the sample to be identified.

Due to the stochastic nature of Brownian motion, the distribution of sizes determined by MSD and the Stokes-Einstein equation will be wider than the real distribution. One way of addressing this is to set a high minimum number of images frames for each track[192]. This can however drastically reduce the number of particles detected. Another strategy is to apply algorithms which estimates the probable real distribution[191, 193], something which has been implemented in more recent versions of commercial NTA software.

Since NTA can, in addition to size, measure the light scattering intensity for individual particles, it can in principle be used to differentiate between particles populations of different refractive index. In practice this is made difficult be non-uniform intensity profile of the laser beam, which gives a non-uniform illumination of the sample in view. Nevertheless, by taking the non-uniform illumination into account in the data analysis, experimental determination of refractive index of different particles has been reported[192, 194, 195]. It is however not possible to differentiate between a positive and a negative difference in refractive index between particle and medium and thus not between gas bubbles and particles/droplets.

A general problem with NTA is that the method is sensitive to camera and image analysis settings, which need to be carefully selected and kept the same between measurements for results to be comparable[196]. The result is also sensitive to the height in the sample at which the microscope is focused, which is a manual setting that is difficult to repeat consistently. Another source of error is that when a particle drift in and out of focus, it's imaged scattering intensity will vary, and it may be tracked several times. This problem is aggravated by the non-uniform intensity of the laser beam[197].

If particles with very different scattering intensities are present, it can be difficult to make a correct measurement. If settings are optimized for the strongest scatterers, the weakest ones might not be visible. If the settings are optimized for the weakest scatterers, the strongest scatterers will be visible as very large spots which are difficult to track and obscures other particles in view. This limits how heterogeneous samples that can accurately be analysed.

Commercially available hardware and software is primarily developed for size determination, and there is room for improvement concerning particle concentration and not the least refractive index determination.

4.3.2 NTA instrument - Nanosight LM10 HS (Malvern)

The instrument consists of a laser scattering microscope including a flow chamber, a syringe pump, a 488nm laser, a sCMOS camera (Hamamatsu C11440-50B) and a PC software (NTA3.2.16). The laser is located inside a laser module with a metal coated glass plate on top. A removable top plate with a second glass plate for viewing is placed on top of the illumination window. The laser beam illuminates the metal coated glass plate from below, and is refracted by the metal coating such that it acquires an approximately horizontal direction inside the sample chamber. The sample is introduced into the sample chamber through a PTFE capillary (1/16" OD (ca 1.5 mm)) with the help of a syringe pump, controlled from the Nanosight software. The sample chamber is disassembled after each measurement session and cleaned with ethanol, MilliQ water and optionally SDS solution. It is also cleaned before assembly. Due to the risk of etching the optical glass, alkaline cleaning liquids should not be used. Due to the limitations of cleaning methods, there is a certain risk of cross-contamination between experiments to be aware of. There is only one sample chamber which all experimenters use.

There are several software settings to adjust for each measurement, both for the video recording and for the subsequent analysis of the video recording. To make different measurements comparable, it is recommended to change the settings as little as possible and stick to a specific protocol.

For the video recording, screen gain and Cameral Level (CL) are adjustable. Screen gain only affects the display, not the actual measurement. Camera Level is (not linearly) related to shutter time and need to be adjusted depending on the scattering intensity of the particles. If CL is too high, the camera will be saturated by the scattered light from some particles. These will be coloured blue on the screen as an indication for the operator. Large and strongly scattering particles will also be displayed and recorded as very large non-circular entities, which the software often will not be able to track. The CL should be set low enough that only a few of the particles are blue, but high enough that all particles are visible. There are also some "advanced settings", Blur, Max Jump Distance, and Min Track length, which are automatically set by the software if not set manually.

For the analysis of the video recording, the main settings are screen gain and detection threshold. The detection threshold setting affects the results substantially. If set too high, large particles will be overrepresented and small ones not detected.

Under advanced settings, a minimum track length can be set. This determines over how many individual frames a track must extend to be included in the output data. Default is "Auto" which means the software decides a suitable threshold (at least 5). In this work, a minimum tracklength of 10 or 20 images has generally been used. This was found to narrow the size distribution as well as limit the number of false detections in some cases.

4.4 Off-axis Digital Holographic Microscopy (DHM)

4.4.1 Introduction

Digital Holographic Microscopy measures the optical field of the sample, which enables, among other things, generation of phase images at different planes as well as quantification of the phase shift. When light passes through a particle with higher refractive index than the surrounding liquid, it will slow down* and acquire a phase difference compared to light not passing the particle. Vice versa, light will pass faster through a particle with a lower refractive index than the surrounding liquid – typically a gas bubble. DHM thus enables detecting gas bubbles in water and directly differentiating them from particles or droplets. The main disadvantage is however that it cannot detect as small particles as darkfield techniques such as NTA and DLS.

There are several microscopy techniques designed to image phase differences rather than light intensity. Analog phase contrast microscopy[198] uses a regular incoherent light source and is a well-established method to image transparent objects such as living cells, which are more difficult to see in focus in a regular bright field image. By creating constructive interference between light scattered by the object and the background light, areas with phase shifted light will appear brighter in the image. Analog phase contrast does however not enable quantification of phase shifts. Frits Zernike was awarded the Nobel prize in Physics in 1953, for the development of this technique.

There are also several different methods for holographic microscopy[199], which will not be reviewed here. Optical Digital Holographic Microscopy was first reported in the 1990s, and had a breakthrough in the 00s due to the increasing availability of better and cheaper digital cameras and laser sources, as well as

computing power. The basic principle of off-axis DHM, as outlined in Fig. 10., is to split a laser beam into two paths, where one passes through the sample (object beam) and one does not (reference beam). The beams are then recombined and create an interference pattern which is recorded by a digital camera. 3D- information and phase information is extracted by subsequent digital processing.

The second beam splitter, which recombines the two beams, is slightly rotated compared to the incoming beams. This causes the light from the two incoming beams to interfere at the camera plane. Without the off-axis configuration, the two beams would not interfere and the information of interest would not be possible to extract from a single image.

The resolution is diffraction limited, just as in a regular optical microscope. This means that two particles separated by a distance which is less than about half the wavelength of the illuminating light cannot be resolved. Individual light scattering particles of smaller size than that can in principle still be detected, just like in NTA. In particular, some particles can be more easily observed in the phase image than in the bright field image. However, whereas NTA is a darkfield method with low background noise, DHM is a brightfield method with substantial background noise. The signal/noise ratio is therefore lower, which makes it very difficult to detect very small particles. Monodisperse Polystyrene latex particles (RI=1.59) can currently be imaged in water down to a diameter of 0.25 - 0.3 μm, whereas more weakly scattering particles will have a somewhat higher detection limit.

4.4.2 Off-axis Digital Holographic Microscopy – experimental setup

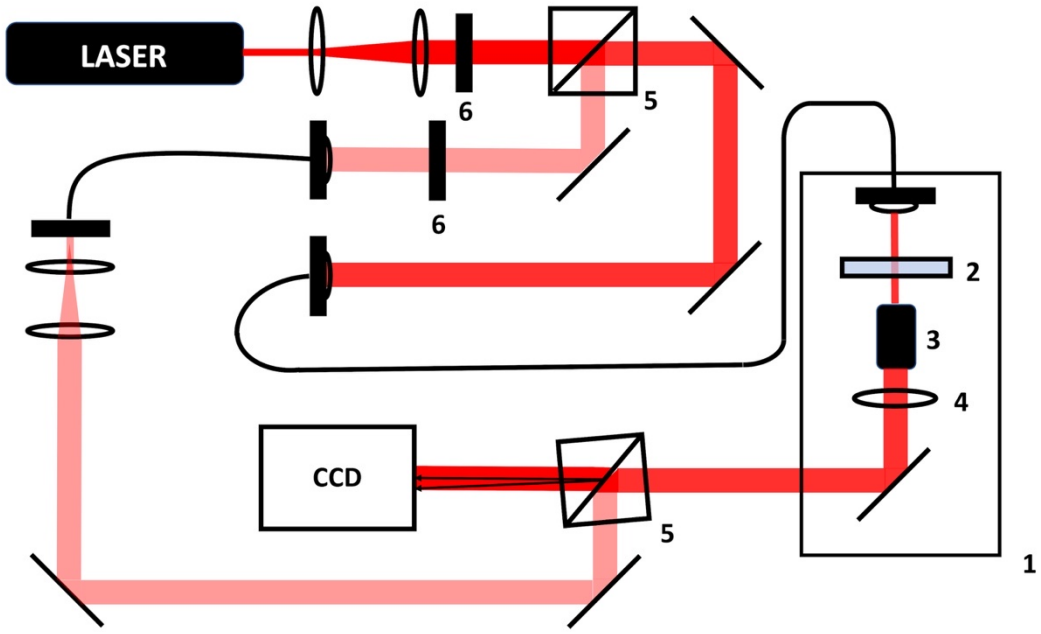

Fig. 10. Digital Holographic Microscope set-up. 1. Inverted microscope, 2. Microfluidic chip/sample, 3. Objective, 4. Tube lens, 5. Beam splitter, 6. Half-wave plate.

The holographic setup is built around a regular inverted microscope (Nikon TE2000-E). The beam from a HeNe laser (633 nm, Newport) is split into two paths, an object beam and a reference beam. The object beam enters an optical fiber which via a collimator illuminates the sample from above. After having passed through the sample, the object beam enters a microscope objective (Olympus, 40x, NA1.30 (oil)) and a tube lens before it exits the microscope to be recombined with the reference beam at a beam splitter close to the front of the CCD-camera (AlliedVision, ProSilica GX1920). In addition, after exiting the laser, the beam is expanded and passed through a half-wave plate before being split by the polarizing beam splitter. The polarizing beam splitter separates the beam into two beams with orthogonal polarization. The light emitted by the laser is already linearly polarized. By adjusting the angle of the polarization before the beam hits the beam splitter, the relative intensity of the two beams can be adjusted. A second half-wave plate in the reference beam path is used to adjust the polarization so that it is the same as that of the object beam when they subsequently meet and interfere. The experimental set-up and hologram construction has also been described paper 2[200] as well as previously[201].

The image is displayed and recorded in avi format by a custom script in LabVIEW (National Instruments). Frame rate and exposure time is selected in the script's user interface. The camera allows frame rates of up to 40 frames per second (fps), normally 20 - 30 fps is used. Exposure times of 2 - 5 ms are normally used. The exposure time is set as high as possible without oversaturating the image. At 30 fps, there is only room for maximum 33 ms exposure time, but another important limitation is that the particle should not move too far during exposure, causing a distorted image. Such distortion can be compensated for in the analysis, but at 2 - 5 ms this is not necessary.

Particle/bubble dispersions are imaged in a channel with the dimensions 20x800 µm, in a microfluidic chip made of Topas (Cyclic Olefin copolymer) (Chipshop). Samples are generally imaged under flow, since this makes it easier to subtract the background noise in the post-processing. The flow also makes it possible to collect images of a larger number of particles. A flow can be achieved by keeping a higher liquid level in the entrance port of the chip than in the exit port. One or a few mm height difference is enough to provide a sufficient pressure difference to drive the flow. The chip can also be connected via a PTFE capillary to a syringe pump to control the flow. Particle/bubble dispersions are also imaged between two clean glass slides, preferably with a distance of 10 µm PTFE film in between. The clean glass gives a somewhat higher image quality, but does not enable a controlled flow and does not contain the sample well.

4.4.3 Off-axis Digital Holographic Microscopy – post-processing

From the avi video file, images of both phase shift type as well as regular bright field images can be created from the measured optical field. It is possible to digitally focus in the image and create an entire stack of images from different focus depths. There are several possible strategies to determine size and RI of the particles. In this work the size is determined from the Brownian motion of the particles and the RI from the size combined with the integrated phase shift. It is also possible to determine size and RI directly from the optical field, something which was demonstrated very recently[202] by using neural networks. The later strategy was shown to give considerably higher accuracy from short tracks, allowing even detection of sub-second size fluctuations of particle agglomerates within the same track. For the very smallest detectable particles (< 300 nm diameter), size detection from Brownian motion does however give less spread.

An overview of the post-processing steps is given in Fig. 12. First, the optical field is extracted using standard methods[203]. The off-axis configuration creates an interference which is visible as fine lines in the bright-field image (Fig. 11a). A Fourier transform of the image will generate three separate Fourier images in one (Fig. 11b.). Without the off-axis configuration these three images would be in the same spot and the information could not be extracted from a single image. The phase information is available in the two outer Fourier images, but not in the center image. By numerically shifting one of the side images to the centre and applying a low pass filter to remove the other two, the information is separated and an inverse Fourier transform can extract the optical field.

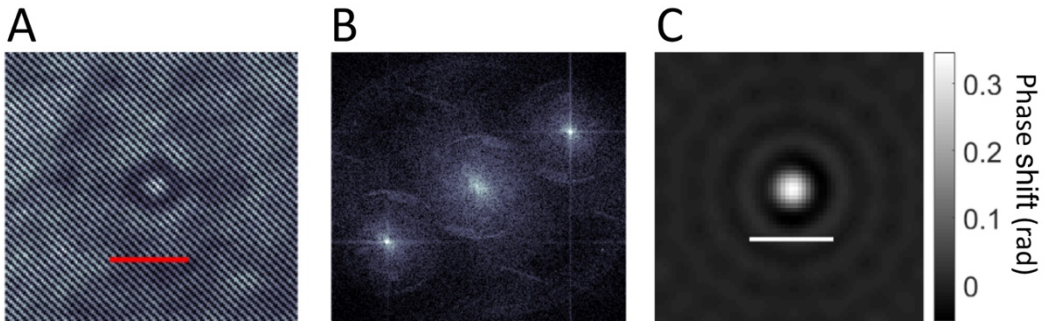

Fig. 11. A: Interference pattern in the bright field image, B: Fourier transform of the bright field image gives three separate Fourier images. C: Filtering out one of the Fourier images which contains the field information, and reverse transforming, a phase shift image can be generated. The scale bar is 2 μm.

Due to optical imperfections, the phase of the retrieved image/field is not uniform. These phase aberrations are fitted to a 4th order polynomial and numerically subtracted from the field. Due to dust and reflections in the optical path, the image contains much spatial noise which drowns much of the optical signal from dispersed particles. Since dirt and reflections are stationary and the dispersion is flowing, the background can be removed by subtracting a previous or later image. However, vibrations cause fluctuations in the image brightness which makes subtraction of an arbitrary single background image insufficient. Since DHM is an interferometric technique, it is very sensitive to vibrations. Furthermore, when subtracting image frames close in time, “ghost particles” with opposite phase shift will appear close to the particles in the image and disturb their optical signal. To handle these problems, the most suitable images frames to subtract are selected from a list of candidates which include frame 10 - 25 after the image and 10 - 25 before the image.

Next, a stack of fields is created for each image by propagating the field to different planes, 2 μm apart, along the optical axis. Subsequently, particles are identified in a maximum intensity projection of the entire field and assigned to one of the axial planes. Following detection and positioning, a more accurate axial position determination is performed by propagating a region of interest 64x64 pixels around each particle to 200 different axial planes, 5 nm apart, and determine at which plane the particle is perfectly in focus.

Many of the detected particles are ghost particles which are due to the background subtraction, these need to be removed from the analysis. Ghost particles have opposite their real phase shift, but they will also appear to emit light rather than scatter light, the later property allows to distinguish them from real particles.

Detected particles are subsequently linked into tracks. For each track the flow speed is estimated, and the current estimated position calculated based on the position in the previous frame. By minimizing the sum of the distances between the positions of detections in the current frame and the estimated positions based on previous frames, the detections are linked together into tracks.

The diffusivity is estimated by analysing the particles horizontal movement perpendicular to the flow direction. In principle it would be advantageous to use movement in three dimensions, since it would give a more accurate diffusivity estimate. However, the movement in the flow direction is difficult to determine since it is hard to determine the flow speed for each individual particle. Furthermore, the position accuracy in the axial direction is lower than in the image plane and it is therefore better to not use the movement in axial direction. The mean square displacement is therefore only estimated in one dimension.

From the diffusivity, the particle size can be determined with the help of the Stokes-Einstein equation. Due to the stochastic nature of Brownian motion, the distribution of diffusivities and thus size distribution will appear wider than it actually is. To limit this broadening of the distribution, the minimum track length is normally set to 10 or 20 frames.

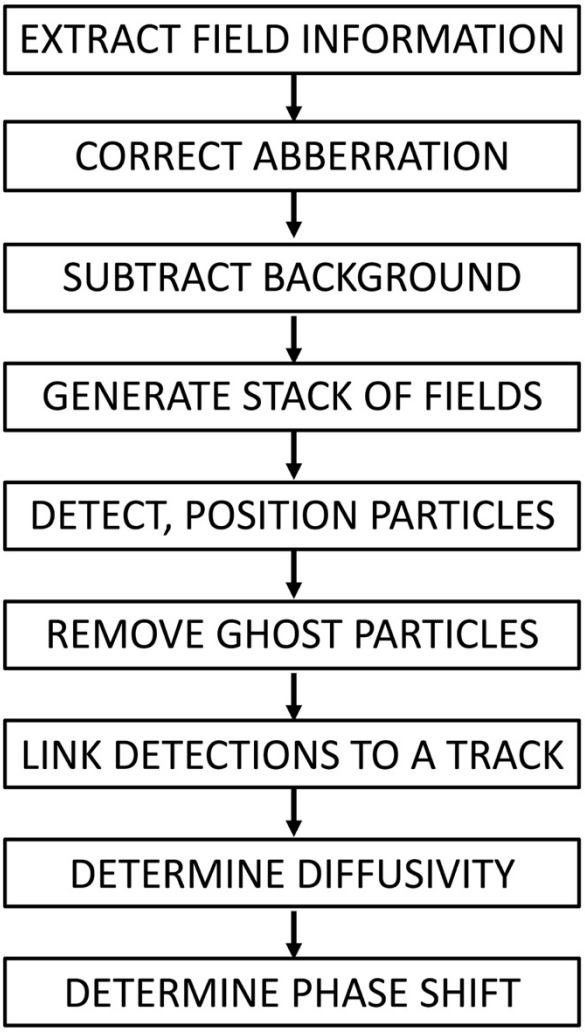

Fig. 12. Post-processing overview.

The integrated phase shift, Φ [rad·μm^2], is the phase shift ϕ [rad] of the light passing the particle, integrated over the projected area of the particle. The integrated phase shift of each particle is determined from a phase image by fitting the particle to a gaussian function. By averaging over all images along the track for the particle, a more accurate value is achieved. For a spherical macroscopic particle, Φ depends on particle volume V, the difference in refractive index Δn between the particle and the dispersion medium, and the wavelength λ as follows:

$$\Phi = \frac{2\pi\Delta n V}{\lambda}$$

For particles in the Mie scattering region, this relation will however need to be adjusted with the help of Mie simulations. Note that inaccuracy in size

determination will translate into inaccuracy in RI. Size and refractive index are thus not independent variables. Calculated RI values for individual particles will thus spread much more than integrated phase shift. It is therefore more useful to plot integrated phase shift against size to resolve different particle populations. Subsequently it can be evaluated how this translates to RI with the help of Mie simulations. As we demonstrate in paper II, if the calculated RI based on assuming the particles to be solid and spherical is different than expected, other assumptions can be evaluated.

The method is computationally heavy, and despite utilizing the strength of parallel computing on a graphics card (Nvidia GTX1080), a single 60 s film (1440x1920 pixels) can take 1-3 h to process depending on particle concentration and settings. The rapid development of GPU technology as well as software optimization can however be expected to make much faster processing possible in the future.

4.5 Particle / bubble differentiation by pressure and vacuum treatment

4.5.1 Pressure

As discussed in chapter 3.7, pressure treatment of a solution can be used in combination with a light scattering method to differentiate between bubbles, which are destroyed by pressure treatment, from solid particles and droplets which are not.

Two different pressure vessels were used for pressure treatment of samples. The first is a plastic vessel, intended to hold water filtration cartridges. This is the same vessel which has been used for hydrodynamic cavitation experiments (see Chapter 5). It is connected to pressurized air, and equipped with a 2μm stainless steel filter (Swagelok) on the inlet. The outlet is equipped with a needle valve, enabling different rates of pressure release. Generally, liquid samples of 1.5 cm depth were exposed to 5 bar pressure for 10 minutes.

The second pressure vessel is a thick-walled stainless-steel cylinder, with internal diameter 31 mm and height 105 mm. The inlet is connected to a tube of compressed Nitrogen, equipped with a high-pressure regulator which can provide a regulated pressure of up to 50 bar. The outlet from the steel cylinder is equipped with a needle valve (Swagelok) which is narrow enough to avoid a too violent pressure release, but does not allow for very slow decompression.

4.5.2 Vacuum

As discussed in chapter 3.8, vacuum can be used to decrease the concentration of dissolved gas in a liquid sample, which will cause bubbles to dissolve. In combination with a light scattering method it can thus be used to differentiate between particles and bubbles.

A digitally controlled vacuum pump (Büchi) was connected to a large vacuum safe glass cylinder. The sample was placed in an 8 mm glass tube and the liquid depth was about 1.5 cm. The pressure was set to 0.1 bar and kept for 24h.

4.6 Dissolved oxygen

Since oxygen is chemically reactive, it is considerably easier to measure its concentration in water than for the more inert nitrogen. There are several methods to determine oxygen concentration in water, for example by Winkler titration or by digital instruments with electrochemical or optical probes. In this work an optical probe, ProOdo from YSI, was used. Before each measurement, the calibration was checked by a measurement in water saturated air.

5 Bubble preparation

5.1 Overview

Many methods have been devised for generating micro- and nanobubbles. They can broadly be divided into dispersion-based and oversaturation-based methods. Dispersion of gas into water can take place by injecting gas through nozzles or membranes, through high-speed stirring, through shaking, etc. Oversaturation can be achieved by saturating water at high pressure and subsequently release the pressure, by saturating water at a lower temperature and subsequently increase the temperature, through electrolysis, or through chemical decomposition of a gas releasing compound. Oversaturation can also be achieved by changing the chemical composition so that the gas solubility decreases, for example by adding inorganic salts to water or by adding water to ethanol[162]. Many methods are based on cavitation, which can be said to achieve both things. Cavitation releases gas by local sub pressure and is also generating considerable dispersion.

5.2 Hydrodynamic cavitation

Hydrodynamic cavitation is carried out with the help of an equipment assembled as follows, inspired by that described in ([204]): Pressurized air is supplied from a pressure regulator via a flexible hose and passes through a stainless steel particle filter with 0.5 µm pore size and into a plastic pressure vessel. The liquid sample is placed in a glass beaker inside the vessel and the air inlet exits above the liquid surface. The outlet pipe extends almost to the bottom of the glass beaker. The outlet pipe is equipped with a needle valve which makes it possible to vary the outlet flow rate. It is possible to expose the sample to cavitation several times by pouring it back into the first beaker and pressurize the vessel again. By keeping the sample under pressure for an hour, while placed on a shaking table to ensure faster equilibration, the sample is oversaturated with air. The standard procedure is 1h at 3 bar pressure and 70 rpm shaking. This is followed by a discharge through the needle valve opened either 1.5 turns which gives a discharge rate of 0.1 l/s or 2.5 turns which gives a flow rate of 0.2 l/s. With or without oversaturation, there is always visible formation of numerous small bubbles following discharge through the needle valve. The advantage of hydrodynamic cavitation is that it uses comparably little energy compared to ultrasound and is possible to scale up to be used for large volumes.

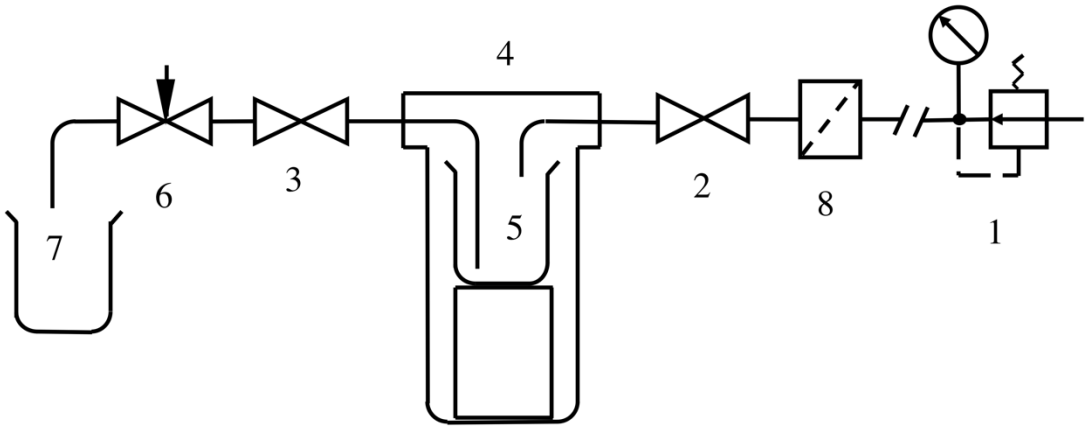

Fig 13. Equipment for hydrodynamic cavitation: (1) Pressure regulator for pressurized air; (2) and (3) Shutoff valves; (4) Pressure vessel; (5) Sample beaker; (6) Needle valve; (7) Outlet beaker; (8) Particle filter

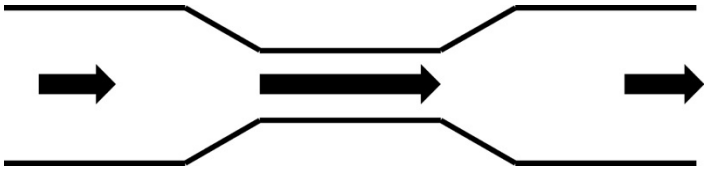

Fig. 14. Technical principle of hydrodynamic cavitation in a constriction. In the wide part, the flow is slower and the pressure is high. In the constriction the flow is faster and the pressure low, causing nucleation of vapor or gas bubbles.

5.3 Probe Sonication

The tip of a sonicator probe (13 mm diameter) is placed at the surface of the liquid sample, immersed only 1-3 mm. The sonicator (Sonics, Vibra-cell) has a maximum power of 500kW and a frequency of 20 kHz. Most often, 30% power (150kW) was used for 30 s. As the probe is placed at the surface, it creates a vigorous stirring of the liquid which entrains and disperses a large amount of air. The position of the probe needs to be carefully adjusted to get much air entrained into the liquid, and the method is therefore somewhat operator dependent. As the probe is used by other experimenters, the risk of cross-contamination is significant. The probe is therefore immersed in NaOH/ethanol solution for a few minutes before sonication, to ensure cleanliness. After this procedure the probe is always well wetted by pure water. Beside the potential for cross-contamination, sonication probes are known to release significant amounts of titanium particles. This has been found to be the case also for this equipment, where a significant concentration of highly light scattering particles were detected after sonication of pure MilliQ water with a thoroughly cleaned probe. Probe sonication delivers much energy into a small

volume of liquid and is thus very efficient, but it is difficult to scale up and consumes much energy.

5.4 Solution mixing

Mixing of two solutions with different concentration of dissolved gas is a very common method to nucleate nanobubbles on flat surfaces[205]. It has also been used for generation of bulk nanobubble in some recent reports, often in nanoparticle dispersions[119, 120] and for nucleation of surface nanobubbles on macroscopic particles[60]. In paper III, solutions equilibrated with air at 4 and 40 °C, respectively were mixed in equal amounts, and the resulting mixture briefly swirled. The resulting solution was at room temperature and had an air oversaturation of 10%. In this case no nanobubbles were detected and there was no visible generation of microbubbles, as is the case with many other nanobubble generation methods. The method has not been used much for nanobubble generation and needs to be investigated further, to find the optimum parameters. The method should be cost-effective and easy to scale up.

5.5 Shaking

A fast and simple method to generate bubbles in the lab is to simply shake the solution in a test tube. This may be less well defined than other methods and less powerful. It does however disperse air into the liquid very efficiently, and does generate quite strong forces in the liquid. It is not seldom used for phospholipid stabilized microbubbles.

As was found in paper I, the stopper can be a source of contamination. Clean PTFE film is therefore used as stopper, firmly pressed against the top of the 8mm glass tube. The tube is shaken as strongly as possible up and down for 30 s.

6 Summary of appended papers

6.1 Paper 1

The first paper presents a selection of the many initial experiments performed which demonstrate the great importance of contaminants in nanobubble research.

Light scattering methods such as DLS and NTA are the most commonly used to detect nanobubbles, but do not actually differentiate between bubbles and droplets or solid particles. Some papers on nanobubbles fail to address this, whereas many others use different complementary techniques to identify bubbles as actual bubbles. We report experiments where hydrodynamic cavitation of pure MilliQ water or pure salt solutions failed to generate any light scattering objects if the equipment was thoroughly cleaned, but did generate light scattering objects if that was not the case. Furthermore, experiments with bubble generation by shaking of MilliQ water or salt solutions in test tubes failed to generate any bubbles but identified several plastic stopper materials as a source of particle contamination. Air nanobubbles in water are commonly reported at concentrations of around 10^8/ml. This may sound like a high number, but for particles as small as 300 nm, this corresponds to a volume fraction of only 1.3 x 10^{-6}. If this volume consists of solid particles with a density of 1.5 g/cm^3 instead of bubbles, it corresponds to 2mg/l. 100nm particles at the same number concentration would have a weight concentration of only 0.08 mg/l.

Experiments were also made with dissolution of very high concentrations (18-22%) of inorganic salts, which generated bubbles by lowering the air solubility in the solution. Light scattering objects were found in all solutions, but were probably mineral particles originating from the salt in most cases. Treatment of the solutions with vacuum and pressure was used to differentiate between bubbles and particles/droplets, since this is expected to destroy bubbles but leave particles unaffected. In one case this treatment did have an effect and thus one solution appeared to actually contain bubbles.

It is pointed out that in the papers which report nanobubbles in pure water or pure salt solutions, adequate contamination control is not reported in any case. Thus, there is no experimental evidence in support of theories on nanobubble stability that is not based on adsorbed impurities. It is concluded that

nanobubbles are most probably stabilized by organic contaminants at small concentrations.

6.2 Paper 2

The second paper demonstrates holographic nanoparticle tracking analysis (H-NTA) for differentiation between bubbles and particles. The bubble preparation was made in a solution of sorbitan-based surfactants (Span/Tween) in 3% NaCl, according to a known protocol. A custom-built off-axis DHM (see chapter 4.4) was used for making video recordings of the sample under flow in a 20μm high channel. Particle size (hydrodynamic diameter) was determined from the diffusivity of the imaged particles, based on tracking of their brownian motion. The phase shift of the light passing the particles was determined and different particle or bubble populations could easily be distinguished in a plot of phase shift vs hydrodynamic diameter. The method was first demonstrated for a mixture of three different polystyrene and silica particles, close in size and refractive index. The three populations, with mean sizes of 0.48, 0.40 and 0.44 μm, and with refractive indices of 1.59, 1.60 and 1.46, could readily be distinguished and their size and refractive index accurately determined. In the bubble preparation, bubbles in the range 0.3-1.5μm were easily distinguished from a population of undissolved surfactant particles, since their phase shift is opposite that of solid particles. Following exposure to 20 bar pressure, the bubbles disappeared completely. This was also the case when the bubbles were diluted in a slightly air undersaturated NaCl solution. This was expected and in line with present understanding of surfactant stabilized bubbles. It was however surprising to find that the apparent refractive index, calculated based on assuming spherical particles, seemed to increase with size to asymptotically approach the refractive index of water. It was concluded that all but the smallest detected bubbles were actually clusters of many individual bubbles. A similar observation has previously been made on bubbles in NaCl solution[121], but it remains to be investigated how universal this phenomenon is. Detecting smaller particle/bubble sizes is unfortunately very challenging, but nevertheless this method was found to be very useful for investigations on nanobubbles.

6.3 Paper 3

In the third paper the dynamic equilibrium model for stable nanobubbles is investigated experimentally (see also chapter 3.4.1). Attempts to generate nanobubbles were made in dispersions of amidine latex (23 nm), mildly

hydrophobized silica (27 nm), graphite (70 nm) and hexadecane droplets. For bubble generation, the solution mixing method was used, where two solutions of different dissolved gas concentration are mixed. This is a common method for surface nanobubble generation and has also been demonstrated for bulk nanobubble generation. Probe sonication was also examined as a bubble generation method. Generation of nanobubbles was evaluated by comparing NTA (Nanoparticle tracking analysis) measurements before and after solution mixing and after 20 bar pressure treatment of the mixed solution. No significant changes could be seen in any case. At least three experiments were made for each particle type. A single set of experiments was also evaluated by H-NTA (Holographic NTA), without detecting any bubbles. In this case the detection limit was however about 250 nm, and bubbles with much adsorbed material, resulting in an effective RI >1.33 would not have been identified as bubbles. Great effort was made to avoid contamination. Glass vials were cleaned with hot alkaline detergent and rinsed with MQ, ethanol and treated with oxygen plasma. When the last ethanol rinse and plasma treatment was omitted in one experiment with positively charged amidine latex, accelerated agglomeration was seen. Presumably this was due to detergent traces on the glass, amidine latex is already well known to be sensitive to anionic contaminants. A handful of recent papers report enhanced nanobubble generation in dispersion of hydrophilic as well as hydrophobic particles and oil droplets. Only one of these does however explicitly relate the results to the dynamic equilibrium model. Based on the contamination sensitivity and particle agglomeration found in the present work, it needs to be considered if some of these results are due to particle agglomerates being mistaken for bubbles.

It has been suggested that oil or fat droplets could act as hydrophobic material in the dynamic equilibrium model. However, hydrocarbon oil does not make out a diffusion barrier, the diffusivity of gas in hydrocarbons is at least as high as in water. Therefore, gas would not diffuse only at the droplet perimeter but also straight through the oil. Solid particles are thus better candidates.

The size of the bubbles predicted by the model vary considerably with the magnitude of the hydrophobic potential, which drives the gas accumulation. The hydrophobic potential is not well known for different surfaces, making this a great uncertainty for the model. It is also noted that the model predicts stable bubbles within a limited parameter space, with maximum four particles adsorbed and minimum 50% surface coverage of the adsorbed particles. Thus, both the model itself as well as the present experiments suggest that bulk

nanobubbles stabilized by dynamic equilibrium are not common and easily achievable. On the other hand, it could be that gas accumulation at hydrophobic surfaces can play a role combined with other stabilization mechanisms such as dense coatings of surfactants, macromolecules or nanoparticles (Pickering emulsion).

6.4 Paper 4

In the fourth paper, the investigations of sorbitan surfactant nanobubbles from paper II were extended, with the objective to gain some general understanding of nanobubble properties and stability mechanisms. Based on suggestions by previous authors[206], it was examined if addition of nanoparticles could improve the stability of nanobubbles. Nanoparticle additions (27 nm silica, with and without surface modifications) did not affect the fresh dispersions, but in several experiments with added nanoparticles the concentration of bubble agglomerates surprisingly continued to increase for 1-2 days. The increasing concentration is presumably due to coalescence and agglomeration of small bubbles below the detection limit, and the particles keep these agglomerates in dispersion by preventing coalescence. A gradual agglomeration on short time scale could in some cases be observed in bubble dispersions without added nanoparticles, as can be seen in Fig. 15.

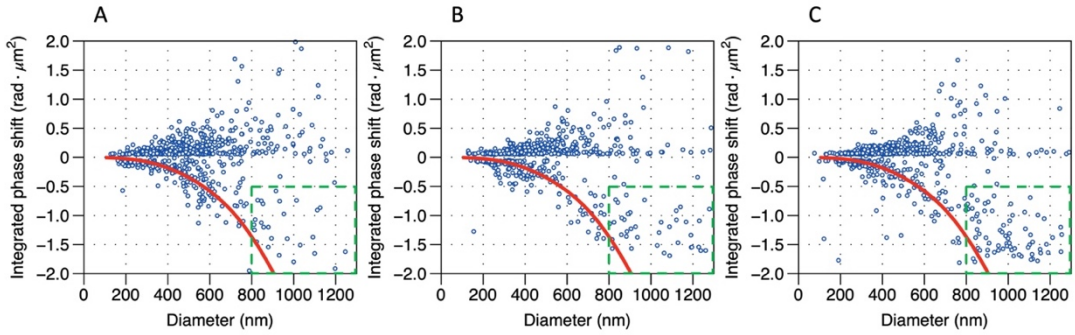

Fig. 15. Bubble dispersion based on Span 60/Tween60 in 3% NaCl, diluted 1:10. Blue circles are detected bubbles or particles. Particles have positive phase shift, bubbles have negative phase shift. The red line shows the expected phase shift for single spherical bubbles with RI=1.00. A gradual agglomeration of bubbles can be seen within the green box, from Panel A (after 17 min), B (after 19 min) to C (after 22 min).

Bubble agglomerates were generally found in the upper part of the microfluidic channel, whereas smaller bubbles were evenly distributed in height, as seen in Fig. 16. Span 60 particles, with a density of close to 1 g/cm^3, were evenly distributed in height, regardless of size. This shows that buoyancy is an important destabilization factor, not only for individual bubbles but also for

agglomerates despite the latter having a small density difference to the surrounding aqueous medium. The buoyancy of bubble agglomerates may potentially have influenced the measurements, as it increases the risk of adsorption in the microfluidic channels.

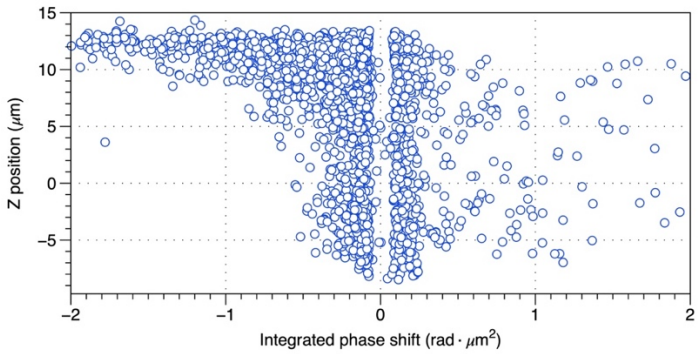

Fig. 16. Height (Z) position in the microfluidic channel for bubbles and particles in st66 dispersion plotted against Integrated phase shift. Optical focus is at Z=0. Small bubbles are evenly distributed in height, whereas larger bubble agglomerates are found exclusively in the upper part of the channel. Particles (right side, positive phase shift) are evenly distributed in height regardless of size. Insoluble Span 60 has a density of 1 g/cm^3.

Regular NTA measurements, with lower size detection limit than H-NTA, showed that the number concentration of Span 60 surfactant particles in the range 70 - 200 nm was orders of magnitude higher than the bubble concentration. These particles likely have a role in preventing coalescence and as a surfactant reservoir, but the main stabilization mechanism is most probably a condensed surfactant monolayer which keeps the surface tension close to zero. It was not possible to generate bubbles when Span 60 (saturated hydrocarbon chain) was exchanged for Span 80 (unsaturated hydrocarbon chain), which is in line with previous reports. A composition with 20% Span 80 did however generate stable nanobubbles, which shows that a certain fraction of unsaturated hydrocarbons chains is acceptable. This is in line with what is found in nature, as natural lung surfactant contains a similar fraction of unsaturated hydrocarbon chains. This paper further demonstrates the usefulness of H-NTA for characterization of bubble dispersions and colloidal dispersions in general. The method can determine not only size and refractive index of dispersed particles, bubbles and droplets, but also fractal dimension of agglomerates, agglomeration rate, and by 3D-position study sedimentation and creaming.

6.5 Additional work

Early work, impurities & surfactants

Extensive experimental work has been performed in this project which is not reported in the four papers. During the early explorative work there was no good method in place to differentiate between bubbles and particles/droplets, which made it very difficult to make stringent analysis of the many preparation methods that were explored. Impurities have been a common issue and the results on this matter reported in paper I is only a selection.

A high-speed stirrer used for bubble generation first appeared to generate nanobubbles. When it was started, it generated a white cloud of microbubbles and light scattering measurements showed remaining submicron particles. However, after repeated use it no longer generated a white cloud of microbubbles and the light scattering measurements showed a lower, barely detectable concentration of particles. Despite thorough cleaning, there was probably some oil on the surface of the stirrer which was released by the strong forces created.

Further, many attempts were made to generate nanobubbles in different solutions of water-soluble surfactants, mostly with negative results. It is now obvious to me that surfactants need to be water insoluble to stabilize nanobubbles, and this is supported by literature on bubbles as well as surface chemistry. However, following this line it has also been found that some poorly soluble surfactants tend to form particles rather than bubbles.

Syringe contamination & cavitation

It was accidentally discovered that water that had been in a certain type of single-use plastic syringes would generate suspected nanobubbles. Water was subsequently drawn in and out of a syringe repeatedly and passed through the hydrodynamic cavitation device (see 5.1) according to standard protocol. NTA measurements showed very low concentration of particles before cavitation, but 10^8-10^9/ml particles of slightly below 100 nm size afterwards. Pressure treatment at 20 bar did not change the size and concentration of the particles, which were probably lubricant droplets from the syringes. Single-use syringes are a well-known source of contamination. Presumably the cavitation broke large (several μm) droplets into small fragments. Alternatively, extremely

small droplets not detectable by NTA, adsorbed on the rapidly shrinking microbubbles generated, where they agglomerated and coalesced.

Bubble generation in natural fresh and sea water

Based on the view that naturally occurring surfactants stabilize nano- and microbubbles, which has indeed been reported by previous authors, samples of natural water were collected for bubble generation. Clear sea water as well as clear yellowish humic-rich fresh water from a forest stream was used. Bubble generation was attempted by, among other things, probe sonication at the water surface. The results were evaluated by NTA combined with pressure treatment, as well as by H-NTA. No evidence of stable bubbles was found. The sonication did however cause agglomeration of particles, which was also clearly visible with a green laser pointer.

Bubble generation in tap- and humic rich fresh water was also attempted by diffusing air through a ceramic membrane, which was a commercial product for nanobubble generation. No evidence of stable bubbles were found by H-NTA or NTA and pressurization.

These are only a small number of non-repeated experiments, but provide another indication that stable bulk nano- and microbubbles is not a general phenomenon, at least in high concentration.

Phospholipid-stabilized bubbles

Some experiments were made with probe sonication of phospholipid-based liposomes. Since air was used as filling gas, the bubbles were not very stable and relatively small concentrations were detected by H-NTA. The time from sonication to measurement were at least 15 min, and air -filled phospholipid bubbles are well known to have short lifetime.

7 Conclusions and outlook

My original plan was to spend a first part of this project on establishing a method to produce nanobubbles and a second part on exploring technical applications for nanobubbles, but soon it became obvious that generation of nanobubbles and unambiguous detection of them was not as straightforward as some literature on the subject had led me to believe. The topic was therefore gradually changed into developing nanobubble detection methods and investigating nanobubble stabilization mechanisms.

Whereas plenty of industrial innovation has focused on mechanical methods to generate nanobubbles, the bubble stabilization mechanism has been more or less ignored. Based on the view that certain impurities in water are necessary for stable nano- and microbubbles to form, finding the right way to control the water chemistry is however more important than equipment design. In the field of micro- and nanobubbles as contrast agents, lipid stabilized bubbles are thoroughly studied and used commercially. However, it is a well-known fact in this field that very high concentrations of lipids (several g/l) are necessary to produce these stable bubbles. How much smaller concentrations of impurities (<10mg/l) can stabilize nanobubbles and what these impurities are remains an unresolved issue, and is an important topic for future research.

Three types of nanobubbles are well established, theoretically and experimentally; lipid/surfactant/particle coated bubbles in the bulk of the liquid, bubbles in pits and crevices on surfaces and on suspended particles, bubbles on top of surfaces and large suspended particles. Several other nanobubble models have been suggested, but besides theoretical objections, the experimental results in this thesis do not support them.

Experimental results within this thesis showed that no stable nanobubbles are formed in very pure water or salt solutions, provided all equipment is thoroughly cleaned beforehand. Similar indications have been reported elsewhere[116, 184, 207]. It could be argued that other bubble generation techniques could have been more successful. However, if nanobubbles can be stabilized by inorganic ions alone, or by the water structure at the air-water interface, then it would be good evidence if nanobubbles were generated in a solution with extremely low concentration of organic contaminants, preferably below 1 ppb. Such low concentrations of organic substances can be quantified with TOC (Total Organic Carbon) analysis. Mass Spectrometry can detect very low concentrations but is not quantitative, and other methods generally lacks the

necessary sensitivity. Furthermore, the bubbles need to be evidenced to be bubbles with more than one appropriate method.

The dynamic equilibrium model, based on the automatic accumulation of gas at hydrophobic surfaces of colloidal particles, is an interesting idea, although the experimental results in this thesis do not support it. Gas accumulation at hydrophobic surfaces is of importance for nanobubbles on surfaces and in crevices, which gives the idea some merit. The present experimental evaluation (paper III) has limitations, it may be that other bubble generation methods and/or other types of nanoparticles are more suitable for generation of bubbles stabilized by such a mechanism. It can also be speculated if the mechanism can be combined with for example surfactant stabilization, which was not tested here. Nevertheless, the model cannot be considered experimentally well evidenced, and there is room for more work both theoretically and experimentally. In its present form, the model predicts bubbles within a rather limited parameter space, a valid model needs to predict bubbles within a wider parameter space.

Many publications on nanobubbles report detection of nanobubbles only by light scattering methods such as DLS and NTA. It is assumed that light scattering nano-objects remaining after vigorous generation of microbubbles are nanobubbles, but this is not with certainty the case. Oil droplets or solid particles may be adsorbed on the shrinking microbubbles, agglomerated and remain after the bubbles have dissolved. It may also be that microbubbles help dislodge impurities from surrounding surfaces. It is possible, perhaps even plausible, that remaining particle agglomerates have crevice bubbles between the individual particles and that such entities are in fact particle/bubble agglomerates. It would however be inappropriate to call such aggregates “nanobubbles” if they are mostly made out of particles. Bubbles within such entities would not necessarily be possible to detect with the two methods used in this thesis (pressurization and holography), but would require other methods of analysis to detect. Chemical analysis of oxygen contents is one possibility, cavitation susceptibility is another.

Bubbles and dissolved gas in water is certainly an interesting topic with many practical implications. Many interesting possibilities are being explored for micro- and nanobubbles within the medical field. Industrially, positive effects of “nanobubble generators” have been reported within for example flotation, agriculture and aquaculture and environmental remediation. However, the positive effects may not necessarily be due to stable bulk nanobubbles, but to

increase in dissolved oxygen, generation of reactive oxygen species (ROS), and nucleation of crevice and surface bubbles on suspended particles. Furthermore, the accumulation of gas at hydrophobic surfaces and the role of dissolved gas for the hydrophobic attraction is a very interesting topic, which may be of underestimated importance in surface chemistry.

Many methods have been suggested in the literature and demonstrated to selectively detect nanobubbles and differentiate them from particles and droplets[102, 116, 124, 159, 169, 171, 185]. Many of these methods have disadvantages. They may be expensive, time-consuming, and in several cases do not produce unambiguous results. We have established two practical and useful methods in this project. The first is measurement of size and concentration with light scattering methods, before and after exposure to high pressure. Bubbles are expected to be destroyed by such treatment, whereas particles or droplets remain unaffected. In this work, pressure treatment was shown to destroy 300 nm large surfactant stabilized bubbles, and pressure treatment to destroy nanobubbles has also been reported by several other authors. It can be considered a relatively established method. There are some minor concerns, the method might itself nucleate bubbles, and there might be a possibility that it can also dissolve slightly water-soluble oil droplets. These concerns should be investigated further, to verify the method. Furthermore, measuring size while simultaneously changing the pressure is a powerful method demonstrated recently[207], which deserves attention.

The second method is holographic nanoparticle tracking analysis (H-NTA), using off-axis Digital Holographic Microscopy (DHM). DHM is not an established method in the nano- and microbubble field, and it is today mostly used for imaging of living cells – not submicron particles. Despite considerable challenges, it is a method with great promise for the future, not only in the field of live-cell imaging but also for the analysis of colloidal dispersions. Although holographic tracking of submicron particles has been demonstrated before[208], using a different technique (inline holography), paper II is the first reported use of off-axis DHM for this purpose. The lower size limit of 250-300 nm is a considerable improvement, which we believe can be advanced further. As opposed to today's work horses in nanoparticle dispersion characterization, such as DLS, NTA and flow cytometry, H-NTA provides information not only about the size and number of particles, but also their refractive index and thereby the composition of particles. As the refractive index of bubbles is lower than that of water whereas virtually all solid materials and oils have a higher

refractive index than water, bubbles can readily be differentiated from other entities.

The technique is heavily dependent on digital computation capacity and the analysis is currently quite time consuming. But with software optimization, for instance by using deep learning, and the rapid development of parallel computing hardware, H-NTA will become increasingly powerful and competitive in the future.

Acknowledgements

I would like to thank my supervisor Jan Swenson, who allowed me to pursue this project under great freedom, while always being available for advice and helping me navigate in the academic world. Your always-reply-within-a-week-policy is a great example for others to follow. Furthermore, my first assistant supervisor Helén Jansson for valuable discussions and great enthusiasm. It is unfortunate you could not be with us through the entire project. Fredrik Höök, assistant supervisor and examiner, for very valuable discussions and scientific mentorship. My present and previous colleagues at Biophysics, where there is a true collaborative spirit and great atmosphere. In particular a great thanks to my enormously talented colleagues Daniel Midtvedt, Erik Olsén and Benjamin Midtvedt for your brilliant development work on the holographic particle tracking technology. Without you this thesis would have looked considerably different. A great thank you to Ezio Zhangelini for much technical help and indefinite loan of the steel pressure chamber. Thanks also to technicians Lennart Norberg and Lasse Urholm, who helped me design and assemble the cavitation device as well as the pressure chamber, and other installation works. Thank you, Romain Bordes (Applied chemistry) for valuable discussions, surfactant samples and use of the probe sonicator. Thank you also to Sanna Björkegren (Applied chemistry/Nouryon) for silica sol samples as well as valuable discussions.

I would like to express my appreciation to the organizers of Nanobubble 2018 conference in beautiful Suzhou and the great hospitality showed. Meeting so many researchers in the same field was very valuable and I had a great time. I also greatly appreciated the ultrasound contrast agent summer school in Boulder, Colorado, (2019) arranged by Mark Borden.

Thank you, all other nice and interesting people I have met at Chalmers and who may have contributed one way or another. And all my friends in the wide world outside Chalmers.

And finally, I would like to thank my parents, for supporting me and believing in me. Without you this would not have happened.

Bibliography

1. Segers, T.; de Jong, N.; Lohse, D.; Versluis, M., Microbubbles for Medical Applications. In *Microfluidics for medical applications*, Royal Society of Chemistry: London, 2014; Vol. 36, pp 81-101.

2. Kiuri, H. J., Development of dissolved air flotation technology from the first generation to the newest (third) one (DAF in turbulent flow conditions). *Water Science and Technology* **2001,** *43* (8), 1-7.

3. Fuerstenau, M. C.; Jameson, G. J.; Yoon, R.-H., *Froth flotation: a century of innovation*. Society for Mining, Metallurgy, and Exploration: Littleton, Colorado, 2007.

4. Zhu, J.; An, H.; Alheshibri, M.; Liu, L.; Terpstra, P. M.; Liu, G.; Craig, V. S., Cleaning with Bulk Nanobubbles. *Langmuir* **2016,** *32* (43), 11203-11211.

5. Ebina, K.; Shi, K.; Hirao, M.; Hashimoto, J.; Kawato, Y.; Kaneshiro, S.; Morimoto, T.; Koizumi, K.; Yoshikawa, H., Oxygen and air nanobubble water solution promote the growth of plants, fishes, and mice. *PLoS One* **2013,** *8* (6), e65339.

6. Zhang, H.; Lyu, T.; Bi, L.; Tempero, G.; Hamilton, D. P.; Pan, G., Combating hypoxia/anoxia at sediment-water interfaces: A preliminary study of oxygen nanobubble modified clay materials. *Sci Total Environ* **2018,** *637-638*, 550-560.

7. Liu, S.; Oshita, S.; Kawabata, S.; Makino, Y.; Yoshimoto, T., Identification of ROS Produced by Nanobubbles and Their Positive and Negative Effects on Vegetable Seed Germination. *Langmuir* **2016,** *32* (43), 11295-11302.

8. Leighton, T. G.; Coles, D. G. H.; Srokosz, M.; White, P. R.; Woolf, D. K., Asymmetric transfer of CO2 across a broken sea surface. *Sci Rep* **2018,** *8* (1), 8301.

9. Schenk, H. J.; Espino, S.; Romo, D. M.; Nima, N.; Do, A. Y.; Michaud, J. M.; Papahadjopoulos-Sternberg, B.; Yang, J.; Zuo, Y. Y.; Steppe, K.; Jansen, S., Xylem Surfactants Introduce a New Element to the Cohesion-Tension Theory. *Plant Physiol* **2017,** *173* (2), 1177-1196.

10. Georgalis, Y.; Kierzek, A. M.; Saenger, W., Cluster formation in aqueous electrolyte solutions observed by dynamic light scattering. *J. Phys. Chem. B* **2000,** *104*, 3405-3406.

11. Samal, S.; Geckeler, K. E., Unexpected solute aggregation in water on dilution. *Chemical Communications* **2001,** (21), 2224-2225.

12. Sedlak, M., Large Supra molecular structure in solutions of low molar mass compounds and mixtures of liquids - I Light scattering characterization. *J. Phys. Chem. B* **2006,** *110*, 4329-4338.

13. Fan Jin, J. L., Xiaodong Ye, Chi Wu, Effects of pH and ionic strength on the stability of nanobubbles in aqueous solutions of a-cyclodextrin. *J. Phys. Chem. B* **2007,** *111*, 11745-11749.

14. Naoyuki Ishida, T. I., Minoru Miyahara, Ko Higashitani, Nano bubbles on a hydrophobic surface in water observed by tapping-mode atomic force microscopy. *Langmuir* **2000,** *16*, 6377-6380.

15. Attard, P., Nanobubbles and the hydrophobic attraction. *Advances in Colloid and Interface Science* **2003,** *104* (1-3), 75-91.

16. Fine bubble industry association - web page. fbia.or.jp.

17. Franc, J.-P.; Michel, J.-M., *Fundamentals of cavitation*. Kluwer Academic Publishers: 2005.

18. Harvey, E. N., Physical factors in bubble formation. In *Decompression sickness*, WB Saunders Co: Philadelphia, 1951.

19. Harvey, E. N.; Barnes, D. K.; McElroy, W. D.; Whiteley, A. H.; Pease, D. C., Removal of gas nuclei from liquids and surfaces *J. Am. Chem. Soc.* **1945,** *67* (1), 156-157.

20. Harvey, E. N.; Barnes, D. K.; McElroy, W. D.; Whiteley, A. H.; Pease, D. C.; Cooper, K. W., Bubble formation in animals. I. Physical factors. *Journal of Cellular and Comparative Physiology* **1944,** *24* (1), 1-22.

21. Fox, F. E.; Herzfeld, K. F., Gas Bubbles with Organic Skin as Cavitation Nuclei. *J. Acoust. Soc. Am.* **1954,** *26* (6), 984-989.

22. Brennen, C. E., *Cavitation and bubble dynamics*. Oxford University Press: New York, 1995; Vol. 44.

23. D'Arrigo, J. S., Physical properties of the nonionic surfactants surrounding gas cavitation nuclei. *The Journal of Chemical Physics* **1979,** *71* (4), 1809-1813.

24. Khoo, M. T.; Venning, J. A.; Pearce, B. W.; Takahashi, K.; Mori, T.; Brandner, P. A., Natural nuclei population dynamics in cavitation tunnels. *Experiments in Fluids* **2020,** *61* (2).

25. Russell, P. S.; Barbaca, L.; Venning, J. A.; Pearce, B. W.; Brandner, P. A., Measurement of nuclei seeding in hydrodynamic test facilities. *Experiments in Fluids* **2020,** *61* (3).

26. Borkent, B. M.; Arora, M.; Ohl, C.-D., Reproducible cavitation activity in water-particle suspensions. *The Journal of the Acoustical Society of America* **2007,** *121* (3), 1406-1412.

27. Yildirim, A.; Chattaraj, R.; Blum, N. T.; Goodwin, A. P., Understanding Acoustic Cavitation Initiation by Porous Nanoparticles: Toward Nanoscale Agents for Ultrasound Imaging and Therapy. *Chem Mater* **2016,** *28* (16), 5962-5972.

28. Bussonniere, A.; Liu, Q.; Tsai, P. A., Cavitation Nuclei Regeneration in a Water-Particle Suspension. *Phys Rev Lett* **2020,** *124* (3), 034501.

29. Glaser, D. A., Some Effects of Ionizing Radiation on the Formation of Bubbles in Liquids. *Physical Review* **1952,** *87* (4), 665-665.

30. Sette, D.; Wanderlingh, F., Nucleation by Cosmic Rays in Ultrasonic Cavitation. *Physical Review* **1962,** *125* (2), 409-417.

31. Hahn, B.; Peacock, R. N., Ultrasonic cavitation induced by neutrons. *Il Nuovo Cimento (1955-1965)* **1963,** *28* (2), 334-340.

32. Iernetti, G., Cavitation Threshold Dependence on Volume. *Acta Acustica united with Acustica* **1971,** *24* (4), 191-196.

33. Liebermann, L., Air Bubbles in Water. *Journal of Applied Physics* **1957,** *28* (2), 205-211.

34. Craig, V. S. J.; Ninham, B. W.; Pashley, R. M., Direct Measurement of Hydrophobic Forces: A Study of Dissolved Gas, Approach Rate, and Neutron Irradiation. *Langmuir* **1999,** *15* (4), 1562-1569.

35. Chang, H., When water does not boil at the boiling point. *Endeavour* **2007,** *31* (1), 7-11.

36. Blatteau, J.-E.; Souraud, J.-B.; Gempp, E.; Boussuges, A., Gas Nuclei, Their Origin, and Their Role in Bubble Formation. *Aviation, Space, and Environmental Medicine* **2006,** *77* (10), 1068-1076.

37. Arieli, R.; Marmur, A., Evolution of bubbles from gas micronuclei formed on the luminal aspect of ovine large blood vessels. *Respir Physiol Neurobiol* **2013,** *188* (1), 49-55.

38. Yount, D. E.; Strauss, R. H., Bubble formation in gelatin: A model for decompression sickness. *Journal of Applied Physics* **1976,** *47* (11), 5081-5089.

39. Yount, D.; Gillary, E.; Hoffman, D., A microscopic investigation of bubble formation nuclei. *J Acoust Soc Am* **1984,** *76* (5), 1511-1521.

40. Yount, D. E., On the Elastic Properties of the Interfaces That Stabilize Gas Cavitation Nuclei. *Journal of Colloid and Interface Science* **1997,** *193* (1), 50-59.

41. D'Arrigo, J. S., Biological surfactants stabilizing natural microbubbles in aqueous media. *Advances in Colloid and Interface Science* **1983,** *19*, 253-307.

42. Yount, D. E.; Yeung, C. M.; Ingle, F. W., Determination of the radii of gas cavitation nuclei by filtering gelatin. *The Journal of the Acoustical Society of America* **1979,** *65* (6), 1440-1450.

43. *Advances in Echo Imaging using Contrast Enhancement*. Kluwer Academic Publishers: 1993.

44. Wheatley, M. A.; Cochran, M., Ultrasound contrast agents. *Journal of Drug Delivery Science and Technology* **2013,** *23* (1), 57-72.

45. de Jong, N.; Emmer, M.; van Wamel, A.; Versluis, M., Ultrasonic characterization of ultrasound contrast agents. *Med Biol Eng Comput* **2009,** *47* (8), 861-73.

46. Frinking, P.; Segers, T.; Luan, Y.; Tranquart, F., Three Decades of Ultrasound Contrast Agents: A Review of the Past, Present and Future Improvements. *Ultrasound in Medicine & Biology* **2020**.

47. Hernandez, C. Stabilized nanobubbles for diagnostic applications. Diss. Case Western Reserve University, 2018.

48. Xu, X.; Song, R.; He, M.; Peng, C.; Yu, M.; Hou, Y.; Qiu, H.; Zou, R.; Yao, S., Microfluidic production of nanoscale perfluorocarbon droplets as liquid contrast agents for ultrasound imaging. *Lab Chip* **2017,** *17* (20), 3504-3513.

49. Li, J.; Tian, Y.; Shan, D.; Gong, A.; Zeng, L.; Ren, W.; Xiang, L.; Gerhard, E.; Zhao, J.; Yang, J.; Wu, A., Neuropeptide Y Y1 receptor-mediated biodegradable photoluminescent nanobubbles as ultrasound contrast agents for targeted breast cancer imaging. *Biomaterials* **2017,** *116*, 106-117.

50. Churchman, A. H.; Mico, V.; de Pablo, J. G.; Peyman, S. A.; Freear, S.; Evans, S. D., Combined flow-focus and self-assembly routes for the formation of lipid stabilized oil-shelled microbubbles. *Microsystems & Nanoengineering* **2018,** *4*, 17087.

51. Stride, E.; Segers, T.; Lajoinie, G.; Cherkaoui, S.; Bettinger, T.; Versluis, M.; Borden, M., Microbubble Agents: New Directions. *Ultrasound in Medicine & Biology* **2020**.

52. Xiao, W.; Ke, S.; Quan, N.; Zhou, L.; Wang, J.; Zhang, L.; Dong, Y.; Qin, W.; Qiu, G.; Hu, J., The Role of Nanobubbles in the Precipitation and Recovery of Organic-Phosphine-Containing Beneficiation Wastewater. *Langmuir* **2018,** *34* (21), 6217-6224.

53. Temesgen, T.; Bui, T. T.; Han, M.; Kim, T. I.; Park, H., Micro and nanobubble technologies as a new horizon for water-treatment techniques: A review. *Adv Colloid Interface Sci* **2017,** *246*, 40-51.

54. Nazari, S.; Shafaei, S. Z.; Gharabaghi, M.; Ahmadi, R.; Shahbazi, B., Effect of frother type and operational parameters on nano bubble flotation of quartz coarse particles. *Journal of Mining & Environment* **2017**.

55. Knüpfer, P.; Ditscherlein, L.; Peuker, U. A., Nanobubble enhanced agglomeration of hydrophobic powders. *Colloids Surf, A* **2017,** *530* (Supplement C), 117-123.

56. Calgaroto, S.; Azevedo, A.; Rubio, J., Flotation of quartz particles assisted by nanobubbles. *Int. J. Miner. Proc.* **2015,** *137*, 64-70.

57. Wang, Y.; Pan, Z.; Jiao, F.; Qin, W., Understanding bubble growth process under decompression and its effects on the flotation phenomena. *Minerals Engineering* **2020,** *145*.

58. Zhou, W.; Wu, C.; Lv, H.; Zhao, B.; Liu, K.; Ou, L., Nanobubbles heterogeneous nucleation induced by temperature rise and its influence on minerals flotation. *Applied Surface Science* **2020**.

59. Ding, S.; Xing, Y.; Zheng, X.; Zhang, Y.; Cao, Y.; Gui, X., New Insights into the Role of Surface Nanobubbles in Bubble-Particle Detachment. *Langmuir* **2020,** *36* (16), 4339-4346.

60. Wang, Y.; Pan, Z.; Luo, X.; Qin, W.; Jiao, F., Effect of nanobubbles on adsorption of sodium oleate on calcite surface. *Minerals Engineering* **2019,** *133*, 127-137.

61. Nazari, S.; Chehreh Chelgani, S.; Shafaei, S. Z.; Shahbazi, B.; Matin, S. S.; Gharabaghi, M., Flotation of coarse particles by hydrodynamic cavitation generated in the presence of conventional reagents. *Separation and Purification Technology* **2019,** *220*, 61-68.

62. Zhou, W.; Niu, J.; Xiao, W.; Ou, L., Adsorption of bulk nanobubbles on the chemically surface-modified muscovite minerals. *Ultrason Sonochem* **2019,** *51*, 31-39.

63. Azevedo, A.; Oliveira, H.; Rubio, J., Bulk nanobubbles in the mineral and environmental areas: Updating research and applications. *Adv Colloid Interface Sci* **2019,** *271*, 101992.

64. Pourkarimi, Z.; Rezai, B.; Noaparast, M., Effective parameters on generation of nanobubbles by cavitation method for froth flotation applications. *Physicochem. Probl. Miner. Process.* **2017,** *53* (2), 920−942.

65. Fan, M.; Tao, D.; Honaker, R.; Luo, Z., Nanobubble generation and its application in froth flotation (part I): nanobubble generation and its effects on properties of microbubble and millimeter scale bubble solutions. *Mining Science and Technology (China)* **2010,** *20* (1), 1-19.

66. Zhou, Z. A.; Xu, Z.; Finch, J. A.; Hu, H.; Rao, S. R., Role of hydrodynamic cavitation in fine particle flotation. *International Journal of Mineral Processing* **1997,** *51* (1), 139-149.

67. Edzwald, J. K., Dissolved air flotation and me. *Water Res* **2010,** *44* (7), 2077-106.

68. Liu, Y.; Zhou, Y.; Wang, T.; Pan, J.; Zhou, B.; Muhammad, T.; Zhou, C.; Li, Y., Micro-nano bubble water oxygation: Synergistically improving irrigation water use efficiency, crop yield and quality. *Journal of Cleaner Production* **2019,** *222*, 835-843.

69. Shi, W.; Pan, G.; Chen, Q.; Song, L.; Zhu, L.; Ji, X., Hypoxia Remediation and Methane Emission Manipulation Using Surface Oxygen Nanobubbles. *Environ Sci Technol* **2018,** *52* (15), 8712-8717.

70. Wang, L.; Miao, X.; Ali, J.; Lyu, T.; Pan, G., Quantification of Oxygen Nanobubbles in Particulate Matters and Potential Applications in Remediation of Anaerobic Environment. *ACS Omega* **2018,** *3* (9), 10624-10630.

71. Takahashi, M.; Chiba, K.; Li, P., Free-radical generation from collapsing microbubbles in the absence of dynamic stimulus. *J. Phys. Chem. B* **2006,** *111*, 1343-1347.

72. Yasui, K.; Tuziuti, T.; Kanematsu, W., Mysteries of bulk nanobubbles (ultrafine bubbles); stability and radical formation. *Ultrasonics Sonochemistry* **2018,** *48*, 259-266.

73. Jin, J.; Wang, R.; Tang, J.; Yang, L.; Feng, Z.; Xu, C.; Yang, F.; Gu, N., Dynamic tracking of bulk nanobubbles from microbubbles shrinkage to collapse. *Colloids and Surfaces A: Physicochemical and Engineering Aspects* **2020**, 124430.

74. Pryor, W. A.; Houk, K. N.; Foote, C. S.; Fukuto, J. M.; Ignarro, L. J.; Squadrito, G. L.; Davies, K. J., Free radical biology and medicine: it's a gas, man! *Am J Physiol Regul Integr Comp Physiol* **2006,** *291* (3), R491-511.

75. Epstein, P. S.; Plesset, M. S., On the Stability of Gas Bubbles in Liquid-Gas Solutions. *J. Chem. Phys.* **1950,** *18* (11), 1505-1509.

76. Higgins, P., Environmental Dissolved Oxygen Values Above 100% Air Saturation. www.ysi.com, 2014.

77. Duncan, P. B.; Needham, D., Test of the Epstein-Plesset Model for Gas Microparticle Dissolution in Aqueous Media: Effect of Surface Tension and Gas Undersaturation in Solution. *Langmuir* **2004,** *20*, 2567-2578.

78. Kronberg, B.; Holmberg, K.; Lindman, B., *Surface chemistry of surfactants and polymers*. John Wiley & Sons: 2014.

79. Israelachvili, J. N., *Intermolecular and surface forces*. 2. ed. ed.; Academic Press: 1992.

80. Björkegren, S. Exploring functionalization of colloidal silica for nanoparticle-stabilized emulsions. Chalmers Tekniska Hogskola (Sweden), 2019.

81. Yount, D. E., Skins of varying permeability: A stabilization mechanism for gas cavitation nuclei. *The Journal of the Acoustical Society of America* **1979,** *65* (6), 1429-1439.

82. Crane, J. M.; Hall, S. B., Rapid Compression Transforms Interfacial Monolayers of Pulmonary Surfactant. *Biophysical Journal* **2001,** *80* (4), 1863-1872.

83. Möhwald, H., Chapter 4 - Phospholipid Monolayers. In *Handbook of Biological Physics*, Lipowsky, R.; Sackmann, E., Eds. North-Holland: 1995; Vol. 1, pp 161-211.

84. Kaganer, V. M.; Möhwald, H.; Dutta, P., Structure and phase transitions in Langmuir monolayers. *Reviews of Modern Physics* **1999,** *71* (3), 779-819.

85. Kwan, J. J.; Borden, M. A., Lipid monolayer collapse and microbubble stability. *Adv. Colloid Interface Sci.* **2012,** *183-184* (Supplement C), 82-99.

86. Segers, T.; Lohse, D.; Versluis, M.; Frinking, P., Universal Equations for the Coalescence Probability and Long-Term Size Stability of Phospholipid-Coated Monodisperse Microbubbles Formed by Flow Focusing. *Langmuir* **2017,** *33* (39), 10329-10339.

87. Gopal, A.; Lee, K. Y. C., Headgroup Percolation and Collapse of Condensed Langmuir Monolayers. *The Journal of Physical Chemistry B* **2006,** *110* (44), 22079-22087.

88. Alheshibri, M.; Craig, V. S. J., Armoured Nanobubbles; Ultrasound Contrast Agents Under Pressure. *Journal of Colloid and Interface Science* **2018**.

89. Mountford, P. A.; Sirsi, S. R.; Borden, M. A., Condensation phase diagrams for lipid-coated perfluorobutane microbubbles. *Langmuir* **2014,** *30* (21), 6209-18.

90. Wang, W.; Moser, C. C.; Wheatley, M. A., Langmuir Trough Study of Surfactant Mixtures Used in the Production of a New Ultrasound Contrast Agent Consisting of Stabilized Microbubbles. *J. Phys. Chem.* **1996,** *100*, 13815-13821.

91. Kilic, S.; Bolukcu, E. S., Phase behavior of DSPC/PEG40St mixtures at higher emulsifier contents. *Colloids Surf B Biointerfaces* **2018,** *171*, 368-376.

92. Borden, M. A.; Pu, G.; Runner, G. J.; Longo, M. L., Surface phase behavior and microstructure of lipid/PEG-emulsifier monolayer-coated microbubbles. *Colloids and Surfaces B: Biointerfaces* **2004,** *35* (3), 209-223.

93. Keating, E.; Zuo, Y. Y.; Tadayyon, S. M.; Petersen, N. O.; Possmayer, F.; Veldhuizen, R. A., A modified squeeze-out mechanism for generating high surface pressures with pulmonary surfactant. *Biochim Biophys Acta* **2012,** *1818* (5), 1225-34.

94. Kovalenko, A.; Polavarapu, P.; Pourroy, G.; Waton, G.; Krafft, M. P., pH-controlled microbubble shell formation and stabilization. *Langmuir* **2014,** *30* (22), 6339-47.

95. Cooke, B. D. J. a. R. C., Generation of stabilized microbubbles in seawater. *Science* **1981,** *213* (4504), 209-211.

96. Processes in foaming. In *Bubble and Foam Chemistry*, Pugh, R. J., Ed. Cambridge University Press: Cambridge, 2016; pp 112-154.

97. Andreatta, G.; Lee, L.-T.; Lee, F. K.; Benattar, J.-J., Gas Permeability in Polymer- and Surfactant-Stabilized Bubble Films. *The Journal of Physical Chemistry B* **2006,** *110* (39), 19537-19542.

98. Borden, M. A.; Longo, M. L., Dissolution Behavior of Lipid Monolayer-Coated, Air-Filled Microbubbles: Effect of Lipid Hydrophobic Chain Length. *Langmuir* **2002,** *18*, 9225-9233.

99. Borden, M. A., Lipid-Coated Nanodrops and Microbubbles. In *Handbook of Ultrasonics and Sonochemistry*, 2016; pp 1075-1100.

100. Kim, J. Y.; Song, M. G.; Kim, J. D., Zeta Potential of Nanobubbles Generated by Ultrasonication in Aqueous Alkyl Polyglycoside Solutions. *J Colloid Interface Sci* **2000,** *223* (2), 285-291.

101. Cho, S.-H.; Kim, J.-Y.; Chun, J.-H.; Kim, J.-D., Ultrasonic formation of nanobubbles and their zeta-potentials in aqueous electrolyte and surfactant solutions. *Colloids Surf., A* **2005,** *269* (1-3), 28-34.

102. Nirmalkar, N.; Pacek, A. W.; Barigou, M., On the Existence and Stability of Bulk Nanobubbles. *Langmuir* **2018,** *34* (37), 10964-10973.

103. Uchida, T.; Liu, S.; Enari, M.; Oshita, S.; Yamazaki, K.; Gohara, K., Effect of NaCl on the Lifetime of Micro- and Nanobubbles. *Nanomaterials (Basel)* **2016,** *6* (2).

104. Takahashi, M., Z potential of microbubbles in aqueous solutions - electrical properties of the gas-water interface. *J. Phys. Chem. B* **2005,** *109*, 21858-21864.

105. Ahmed, A. K. A.; Sun, C.; Hua, L.; Zhang, Z.; Zhang, Y.; Zhang, W.; Marhaba, T., Generation of nanobubbles by ceramic membrane filters: The

dependence of bubble size and zeta potential on surface coating, pore size and injected gas pressure. *Chemosphere* **2018,** *203*, 327-335.

106. Thurman, E. M., *Organic Geochemistry Of Natural Waters*. Nijhoff and Junk Inc. : Boston, MA, 1985.

107. Osterroht, C., Extraction of dissolved fatty acids from sea water. *Fresenius J Anal Chem* **1993,** *345*, 773-779.

108. D'Arrigo, J., Chapter 4 - Characteristic Glycopeptide Fraction of Natural Microbubble Surfactant. In *Studies in Interface Science*, D'Arrigo, J., Ed. Elsevier: 2011; Vol. 25, pp 55-80.

109. D'Arrigo, J. S.; Saiz-Jimenez, C.; Reimer, N. S., Geochemical properties and biochemical composition of the surfactant mixture surrounding natural microbubbles in aqueous media. *Journal of Colloid and Interface Science* **1984,** *100*, 96-105.

110. D'Arrigo, J. S., Aromatic proteinaceous surfactants stabilize long-lived gas microbubbles from natural sources. *The Journal of Chemical Physics* **1981,** *75* (2), 962-968.

111. Ruckenstein, E., Nanodispersions of bubbles and oil drops in water. *Colloids and Surfaces A: Physicochemical and Engineering Aspects* **2013,** *423*, 112-114.

112. Chaplin, M. Nanobubbles (ultrafine bubbles). http://www1.lsbu.ac.uk/water/nanobubble.html#r1966 (accessed 6 March 2020).

113. Yasui, K.; Tuziuti, T.; Kanematsu, W.; Kato, K., Dynamic Equilibrium Model for a Bulk Nanobubble and a Microbubble Partly Covered with Hydrophobic Material. *Langmuir* **2016,** *32* (43), 11101-11110.

114. Brenner, M. P.; Lohse, D., Dynamic Equilibrium Mechanism for Surface Nanobubble Stabilization. *Physical Review Letters* **2008,** *101* (21), 214505.

115. Fang, Z.; Wang, L.; Wang, X.; Zhou, L.; Wang, S.; Zou, Z.; Tai, R.; Zhang, L.; Hu, J., Formation and Stability of Surface/Bulk Nanobubbles Produced by Decompression at Lower Gas Concentration. *The Journal of Physical Chemistry C* **2018**.

116. Sugano, K.; Miyoshi, Y.; Inazato, S., Study of Ultrafine Bubble Stabilization by Organic Material Adhesion. *Japanese Journal of Multiphase Flow* **2017,** *31* (3), 299-306.

117. Zhang, M.; Seddon, J. R. T.; Lemay, S. G., Nanoparticle–nanobubble interactions: Charge inversion and re-entrant condensation of amidine latex nanoparticles driven by bulk nanobubbles. *Journal of Colloid and Interface Science* **2019,** *538*, 605-610.

118. Olszok, V.; Rivas-Botero, J.; Wollmann, A.; Benker, B.; Weber, A. P., Particle-induced nanobubble generation for material-selective nanoparticle flotation. *Colloids and Surfaces A: Physicochemical and Engineering Aspects* **2020,** *592*.

119. Xiao, W.; Wang, X.; Zhou, L.; Zhou, W.; Wang, J.; Qin, W.; Qiu, G.; Hu, J.; Zhang, L., The Influence of Mixing and Nano-Solids on the Formation of Nanobubbles. *J Phys Chem B* **2018**.

120. Jannesari, M.; Akhavan, O.; Madaah Hosseini, H. R., Graphene oxide in generation of nanobubbles using controllable microvortices of jet flows. *Carbon* **2018,** *138*, 8-17.

121. Bunkin, N. F.; Shkirin, A. V.; Suyazov, N. V.; Babenko, V. A.; Sychev, A. A.; Penkov, N. V.; Belosludtsev, K. N.; Gudkov, S. V., Formation and Dynamics of Ion-Stabilized Gas Nanobubble Phase in the Bulk of Aqueous NaCl Solutions. *J Phys Chem B* **2016,** *120* (7), 1291-303.

122. Tan, B. H.; An, H.; Ohl, C. D., How Bulk Nanobubbles Might Survive. *Phys Rev Lett* **2020,** *124* (13), 134503.

123. Alheshibri, M.; Qian, J.; Jehannin, M.; Craig, V. S., A History of Nanobubbles. *Langmuir* **2016,** *32* (43), 11086-11100.

124. Ohgaki, K.; Khanh, N. Q.; Joden, Y.; Tsuji, A.; Nakagawa, T., Physicochemical approach to nanobubble solutions. *Chemical Engineering Science* **2010,** *65* (3), 1296-1300.

125. Jin, J.; Feng, Z.; Yang, F.; Gu, N., Bulk Nanobubbles Fabricated by Repeated Compression of Microbubbles. *Langmuir* **2019**.

126. Zhang, X.; Liu, X.; Zhong, Y.; Zhou, Z.; Huang, Y.; Sun, C. Q., Nanobubble Skin Supersolidity. *Langmuir* **2016,** *32* (43), 11321-11327.

127. Ghaani, M. R.; Kusalik, P. G.; English, N. J., Massive generation of metastable bulk nanobubbles in water by external electric fields. *Science Advances* **2020,** *6* (14), eaaz0094.

128. Theodorakis, P. E.; Che, Z., Surface nanobubbles: Theory, simulation, and experiment. A review. *Adv Colloid Interface Sci* **2019,** *272*, 101995.

129. Lohse, D.; Zhang, X., Surface nanobubbles and nanodroplets. *Reviews of Modern Physics* **2015,** *87* (3), 981-1035.

130. Berkelaar, R. P.; Dietrich, E.; Kip, G. A. M.; Kooij, E. S.; Zandvliet, H. J. W.; Lohse, D., Exposing nanobubble-like objects to a degassed environment. *Soft Matter* **2014,** *10*.

131. An, H.; Liu, G.; Craig, V. S., Wetting of nanophases: Nanobubbles, nanodroplets and micropancakes on hydrophobic surfaces. *Adv Colloid Interface Sci* **2015,** *222*, 9-17.

132. Seibert, S.; Klassen, S.; Latus, A.; Bechstein, R.; Kuhnle, A., Origin of Ubiquitous Stripes at the Graphite-Water Interface. *Langmuir* **2020,** *36* (27), 7789-7794.

133. Attard, P., Pinning Down the Reasons for the Size, Shape, and Stability of Nanobubbles. *Langmuir* **2016,** *32* (43), 11138-11146.

134. Tan, B. H.; An, H.; Ohl, C. D., Surface Nanobubbles Are Stabilized by Hydrophobic Attraction. *Phys Rev Lett* **2018,** *120* (16), 164502.

135. Tan, B. H.; An, H.; Ohl, C. D., Stability, Dynamics, and Tolerance to Undersaturation of Surface Nanobubbles. *Phys Rev Lett* **2019,** *122* (13), 134502.

136. Zhou, L.; Wang, X.; Shin, H. J.; Wang, J.; Tai, R.; Zhang, X.; Fang, H.; Xiao, W.; Wang, L.; Wang, C.; Gao, X.; Hu, J.; Zhang, L., Ultrahigh Density of Gas Molecules Confined in Surface Nanobubbles in Ambient Water. *J Am Chem Soc* **2020,** *142* (12), 5583-5593.

137. Zhang, L.; Chen, H.; Li, Z.; Fang, H.; Hu, J., Long lifetime of nanobubbles due to high inner density. *Science in China Series G: Physics, Mechanics and Astronomy* **2008,** *51* (2), 219-224.

138. Strasberg, M., Onset of Ultrasonic Cavitation in Tap Water. *The Journal of the Acoustical Society of America* **1959,** *31* (2), 163-176.

139. Marschall, H. B.; Mørch, K. A.; Keller, A. P.; Kjeldsen, M., Cavitation inception by almost spherical solid particles in water. *Physics of Fluids* **2003,** *15* (2), 545-553.

140. Mørch, K. A., Reflections on cavitation nuclei in water. *Physics of Fluids* **2007,** *19* (7), 072104.

141. Mørch, K. A., Cavitation Nuclei: Experiments and Theory. *Journal of Hydrodynamics, Ser. B* **2009,** *21* (2), 176-189.

142. Borkent, B. M.; Gekle, S.; Prosperetti, A.; Lohse, D., Nucleation threshold and deactivation mechanisms of nanoscopic cavitation nuclei. *Physics of Fluids* **2009,** *21* (10), 102003.

143. Atchley, A. A.; Prosperetti, A., The crevice model of bubble nucleation. *The Journal of the Acoustical Society of America* **1989,** *86* (3), 1065-1084.

144. Thomas, R. G.; Jonnalagadda, U. S.; Kwan, J. J., Biomedical Applications for Gas-Stabilizing Solid Cavitation Agents. *Langmuir* **2019,** *35* (31), 10106-10115.

145. Crum, R. A. R. a. L. A. *THE ROLE OF NUCLEI SIZE IN TRAN'SIENT CAVITATION THRESHOLD MEASUREMENTS*; University of Mississippi: 1984.

146. Israelachvili, J.; Pashley, R., The hydrophobic interaction is long range, decaying exponentially with distance. *Nature* **1982,** *300*, 341.

147. Nguyen, A. V.; Nalaskowski, J.; Miller, J. D.; Butt, H.-J., Attraction between hydrophobic surfaces studied by atomic force microscopy. *International Journal of Mineral Processing* **2003,** *72* (1-4), 215-225.

148. Meyer, E. E.; Lin, Q.; Israelachvili, J. N., Effects of Dissolved Gas on the Hydrophobic Attraction between Surfactant-Coated Surfaces. *Langmuir* **2005,** *21* (1), 256-259.

149. Ducker, W. A.; Mastropietro, D., Forces between extended hydrophobic solids: Is there a long-range hydrophobic force? *Current Opinion in Colloid & Interface Science* **2016,** *22*, 51-58.

150. Ishida, N.; Matsuo, K.; Imamura, K.; Craig, V. S. J., Hydrophobic Attraction Measured between Asymmetric Hydrophobic Surfaces. *Langmuir* **2018**.

151. Schlesinger, I.; Sivan, U., Hydrophobic Repulsion and its Origin. *arXiv:1603.08215* **2016**.

152. Schlesinger, I.; Sivan, U., New Information on the Hydrophobic Interaction Revealed by Frequency Modulation AFM. *Langmuir* **2017,** *33* (10), 2485-2496.

153. Schlesinger, I.; Sivan, U., Three-dimensional characterization of layers of condensed gas molecules forming universally on hydrophobic surfaces. *J Am Chem Soc* **2018**.

154. Uhlig, M. R.; Martin-Jimenez, D.; Garcia, R., Atomic-scale mapping of hydrophobic layers on graphene and few-layer MoS2 and WSe2 in water. *Nat Commun* **2019,** *10* (1), 2606.

155. Wang, Y.; Jiang, Y.; Wang, W., Determining the Subnanometer Thickness of the Water-Depletion Layer at the Interface between Water and the Hydrophobic Substrate. *Anal Chem* **2019,** *91* (18), 11696-11702.

156. Pashley, R. M., Effects of degassing on the formation and stability of surfactant-free emulsions and fine teflon dispersions. *J. Phys. Chem. B* **2003,** *107*, 1714-1720.

157. Pashley, R. M.; Rzechowicz, M.; Pashley, L. R.; Francis, M. J., De-gassed water is a better cleaning agent. *J. Phys. Chem. B* **2005,** *109*, 1231-1238.

158. Aya, N.; Iki, N.; Shimura, T.; Shirai, T.; Tuziuti, T.; Yasui, K.; Kanematsu, W., Measurement of the change in the number of ultrafine bubbles through pressurization. **2014,** *9232*, 92320T.

159. Tuziuti, T.; Yasui, K.; Kanematsu, W., Influence of increase in static pressure on bulk nanobubbles. *Ultrasonics Sonochemistry* **2017,** *38*, 347-350.

160. Waldichuk, M. In *Diffusion of oxygen into still sea water*, OCEAN 75 Conference, 22-25 Sept. 1975; 1975; pp 907-912.

161. Overton, G. D. N.; Williams, P. R.; Trevena, D. H., The influence of cavitation history and entrained gas on liquid tensile strength. *Journal of Physics D: Applied Physics* **1984,** *17* (5), 979.

162. Qiu, J.; Zou, Z.; Wang, S.; Wang, X.; Wang, L.; Dong, Y.; Zhao, H.; Zhang, L.; Hu, J., Formation and Stability of Bulk Nanobubbles Generated by Ethanol-Water Exchange. *ChemPhysChem* **2017**.

163. Tian, J.; Yang, F.; Cui, H.; Zhou, Y.; Ruan, X.; Gu, N., A Novel Approach to Making the Gas-Filled Liposome Real: Based on the Interaction of Lipid with Free Nanobubble within the Solution. *ACS Appl Mater Interfaces* **2015,** *7* (48), 26579-84.

164. Häbich, A.; Ducker, W.; Dunstan, D. E.; Zhang, X., Do stable nanobubbles exist in mixtures of organic solvents and water. *J. Phys. Chem. B* **2010,** *114*, 6962–6967.

165. Sedlak, M.; Rak, D., Large-scale inhomogeneities in solutions of low molar mass compounds and mixtures of liquids: supramolecular structures or nanobubbles? *J Phys Chem B* **2013,** *117* (8), 2495-504.

166. Zhou, C.; Cleland, D.; Snell, J.; Qi, W.; Randolph, T. W.; Carpenter, J. F., Formation of Stable Nanobubbles on Reconstituting Lyophilized Formulations Containing Trehalose. *J Pharm Sci* **2016,** *105* (7), 2249-53.

167. Tuziuti, T.; Yasui, K.; Kanematsu, W., Influence of addition of degassed water on bulk nanobubbles. *Ultrason Sonochem* **2018,** *43*, 272-274.

168. Zhang, X. H.; Li, G.; Maeda, N.; Hu, J., Removal of Induced Nanobubbles from Water/Graphite Interfaces by Partial Degassing. *Langmuir* **2006,** *22* (22), 9238-9243.

169. Hain, N.; Wesner, D.; Druzhinin, S. I.; Schonherr, H., Surface Nanobubbles Studied by Time-Resolved Fluorescence Microscopy Methods Combined with AFM: The Impact of Surface Treatment on Nanobubble Nucleation. *Langmuir* **2016,** *32* (43), 11155-11163.

170. Uchida, T.; Nishikawa, H.; Sakurai, N.; Asano, M.; Noda, N., Ultra-Fine Bubble Distributions in a Plant Factory Observed by Transmission Electron Microscope with a Freeze-Fracture Replica Technique. *Nanomaterials* **2018,** *8* (3), 152.

171. Uchida, T.; Oshita, S.; Ohmori, M.; Tsuno, T.; Soejima, K.; Shinozaki, S.; Take, Y.; Mitsuda, K., Transmission electron microscopic observations of nanobubbles and their capture of impurities in wastewater. *Nanoscale Res Lett* **2011,** *6* (1), 295.

172. Jadhav, A. J.; Barigou, M., Bulk Nanobubbles or Not Nanobubbles: That is the Question. *Langmuir* **2020**.

173. Cochard, H.; Bodet, C.; Améglio, T.; Cruiziat, P., Cryo-Scanning Electron Microscopy Observations of Vessel Content during Transpiration in Walnut Petioles. Facts or Artifacts? *Plant Physiology* **2000,** *124* (3), 1191.

174. Placzek, M.; Kosela, M., Microscopic methods in analysis of submicron phospholipid dispersions. *Acta Pharm* **2016,** *66* (1), 1-22.

175. Huang, T.-W.; Liu, S.-Y.; Chuang, Y.-J.; Hsieh, H.-Y.; Tsai, C.-Y.; Wu, W.-J.; Tsai, C.-T.; Mirsaidov, U.; Matsudaira, P.; Chang, C.-S.; Tseng, F.-G.; Chen, F.-R., Dynamics of hydrogen nanobubbles in KLH protein solution studied with in situ wet-TEM. *Soft Matter* **2013,** *9* (37), 8856-8861.

176. Wang, L.; Liu, L.; Mohsin, A.; Wen, J.; Sheng, H.; Miller, D. J., Dynamic Nanobubbles in Graphene Liquid Cell under Electron Beam Irradiation. *Microscopy and Microanalysis* **2017,** *23* (S1), 866-867.

177. Hoppe, S. M.; Sasaki, D. Y.; Kinghorn, A. N.; Hattar, K., In-situ transmission electron microscopy of liposomes in an aqueous environment. *Langmuir* **2013,** *29* (32), 9958-61.

178. Hirokawa, S.; Teshima, H.; Solis-Fernandez, P.; Ago, H.; Tomo, Y.; Li, Q. Y.; Takahashi, K., Nanoscale Bubble Dynamics Induced by Damage of Graphene Liquid Cells. *ACS Omega* **2020,** *5* (19), 11180-11185.

179. Hain, N.; Handschuh-Wang, S.; Wesner, D.; Druzhinin, S. I.; Schönherr, H., Multimodal Microscopy-Based Identification of Surface Nanobubbles. *Journal of Colloid and Interface Science* **2019**.

180. Oh, S. H.; Kim, J. M., Generation and Stability of Bulk Nanobubbles. *Langmuir* **2017,** *33* (15), 3818-3823.

181. Zhang, X. H.; Khan, A.; Ducker, W. A., A nanoscale gas state. *Phys Rev Lett* **2007,** *98* (13), 136101.

182. Song, L.; Wang, G.; Hou, X.; Kala, S.; Qiu, Z.; Wong, K. F.; Cao, F.; Sun, L., Biogenic nanobubbles for effective oxygen delivery and enhanced photodynamic therapy of cancer. *Acta Biomater* **2020,** *108*, 313-325.

183. Kikuchi, K.; Ioka, A.; Oku, T.; Tanaka, Y.; Saihara, Y.; Ogumi, Z., Concentration determination of oxygen nanobubbles in electrolyzed water. *Journal of Colloid and Interface Science* **2009,** *329* (2), 306-309.

184. Rak, D.; Ovadova, M.; Sedlak, M., On the (non)Existence of Bulk Nanobubbles: The Role of Ultrasonic Cavitation and Organic Solutes in Water. *J Phys Chem Lett* **2019**.

185. Alheshibri, M.; Craig, V. S. J., Differentiating between Nanoparticles and Nanobubbles by Evaluation of the Compressibility and Density of Nanoparticles. *The Journal of Physical Chemistry C* **2018**.

186. Bohren, C. F.; Huffman, D. R., *Absorption and scattering of light by small particles*. Wiley: New York, 1998.

187. Chowdhury, D., 100 years of Einstein's theory of Brownian motion: from pollen grains to protein trains. *Resonance* **2005,** *10* (9), 63-78.

188. Tabor, D., *Gases, liquids and solids and other states of matter*. 3. ed. ed.; Cambridge Univ. Press: 1991.

189. Hassan, P. A.; Rana, S.; Verma, G., Making sense of Brownian motion: colloid characterization by dynamic light scattering. *Langmuir* **2015,** *31* (1), 3-12.

190. Michalet, X., Mean Square Displacement Analysis of Single-Particle Trajectories with Localization Error: Brownian Motion in Isotropic Medium. *Physical review. E, Statistical, nonlinear, and soft matter physics* **2010,** *82* (4 Pt 1), 041914-041914.

191. Saveyn, H.; De Baets, B.; Thas, O.; Hole, P.; Smith, J.; Van der Meeren, P., Accurate particle size distribution determination by nanoparticle tracking analysis based on 2-D Brownian dynamics simulation. *Journal of Colloid and Interface Science* **2010,** *352* (2), 593-600.

192. van der Pol, E.; Coumans, F. A.; Sturk, A.; Nieuwland, R.; van Leeuwen, T. G., Refractive index determination of nanoparticles in suspension using nanoparticle tracking analysis. *Nano Lett* **2014,** *14* (11), 6195-201.

193. Kim, A.; Ng, W. B.; Bernt, W.; Cho, N. J., Validation of Size Estimation of Nanoparticle Tracking Analysis on Polydisperse Macromolecule Assembly. *Sci Rep* **2019,** *9* (1), 2639.

194. Gardiner, C.; Shaw, M.; Hole, P.; Smith, J.; Tannetta, D.; Redman, C. W.; Sargent, I. L., Measurement of refractive index by nanoparticle tracking analysis reveals heterogeneity in extracellular vesicles. *J Extracell Vesicles* **2014,** *3*, 25361.

195. Matsuura, Y.; Nakamura, A.; Kato, H., Novel Approach for Reliable Determination of the Refractive Index of Particles in the Liquid Phase Using a Hybrid Flow Particle Tracking Method. *Anal Chem* **2020,** *92* (8), 5994-6002.

196. Gross, J.; Sayle, S.; Karow, A. R.; Bakowsky, U.; Garidel, P., Nanoparticle tracking analysis of particle size and concentration detection in suspensions of polymer and protein samples: Influence of experimental and data evaluation parameters. *Eur J Pharm Biopharm* **2016,** *104*, 30-41.

197. Block, S.; Fast, B. J.; Lundgren, A.; Zhdanov, V. P.; Hook, F., Two-dimensional flow nanometry of biological nanoparticles for accurate determination of their size and emission intensity. *Nat Commun* **2016,** *7*, 12956.

198. Zernike, F., How I Discovered Phase Contrast. *Science* **1955,** *121* (3141), 345.

199. Kim, M. K., *Digital Holographic Microscopy - Principles, Techniques, and Applications*. Springer: New York, 2011.

200. Midtvedt, D.; Eklund, F.; Olsén, E.; Midtvedt, B.; Swenson, J.; Höök, F., Size and Refractive Index Determination of Subwavelength Particles and Air Bubbles by Holographic Nanoparticle Tracking Analysis. *Analytical Chemistry* **2020,** *92* (2), 1908-1915.

201. Midtvedt, D.; Olsén, E.; Höök, F.; Jeffries, G. D. M., Label-free spatio-temporal monitoring of cytosolic mass, osmolarity, and volume in living cells. *Nature Communications* **2019,** *10* (1), 340.

202. Midtvedt, B.; Olsén, E.; Eklund, F.; Höök, F.; Adiels, C. B.; Volpe, G.; Midtvedt, D., Holographic characterisation of subwavelength particles enhanced by deep learning. arXiv 2006.11154: (submitted), 2020.

203. Kim, M. K., Principles and techniques of digital holographic microscopy. *SPIE Reviews* **2010,** *1*, 1-51.

204. Calgaroto, S.; Wilberg, K. Q.; Rubio, J., On the nanobubbles interfacial properties and future applications in flotation. *Miner. Eng.* **2014,** *60*, 33-40.

205. Li, D.; Qi, L.; Liu, Y.; Bhushan, B.; Gu, J.; Dong, J., Study on the Formation and Properties of Trapped Nanobubbles and Surface Nanobubbles by Spontaneous and Temperature Difference Methods. *Langmuir* **2019,** *35* (37), 12035-12041.

206. Methachan, B. Study of Gas Bubbles Stabilized by Surfactants for Use as Ultrasound Contrast Agents and Drug Carriers. Drexel University, 2012.

207. Alheshibri, M.; Craig, V. S. J., Differentiating between Nanoparticles and Nanobubbles by Evaluation of the Compressibility and Density of Nanoparticles. *The Journal of Physical Chemistry C* **2018,** *122* (38), 21998-22007.

208. Lee, S.-H.; Roichman, Y.; Yi, G.-R.; Kim, S.-H.; Yang, S.-M.; Blaaderen, A. v.; Oostrum, P. v.; Grier, D. G., Characterizing and tracking single colloidal particles with video holographic microscopy. *Optics express* **2007,** *15* (26).